GRADUATE SCHOOL OF URBAN INNOVATION

INFRASTRUCTURE AND URBAN SOCIETY

YOKOHAMA NATIONAL UNIVERSITY

WEATHERING OF MUDSTONE AND ITS EFFECTS ON CUT SLOPE STABILITY

泥岩の風化機構と切土斜面の安定性への影響

SHARMILY BHOWMIK

20WA916

Doctoral Dissertation

SEPTEMBER, 2023

WEATHERING OF MUDSTONE AND ITS EFFECTS ON CUT SLOPE STABILITY

泥岩の風化機構と切土斜面の安定性への影響

by

SHARMILY BHOWMIK

シャーミリー　ボウミック

A Dissertation Submitted to the Graduate School of Urban Innovation, Yokohama National University in Partial Fulfillment of the Requirement for the Degree of

Doctor of Philosophy in Engineering

Yokohama National University, Graduate School of Urban Innovation

Examination Committee

Dr. Mamoru Kikumoto (Chair)

Professor, Geotechnical Laboratory, Yokohama National University

Dr. Kimitoshi Hayano

Professor, Geotechnical Laboratory, Yokohama National University

Dr. Ying Cui

Associate Professor, Geotechnical Laboratory, Yokohama National University

Dr. Takayuki Suzuki

Professor, Estuarine and Coastal Engineering Laboratory, Yokohama National University

Dr. Chikako Fujiyama

Professor, Concrete Laboratory, Yokohama National University

SEPTEMBER, 2023

ACKNOWLEDGEMENT

Firstly, my deepest gratitude goes to my supervisor, Professor Dr Mamoru Kikumoto, without whom this research would have been impossible. His patient guidance, inspiration, and advice, helping me acquire knowledge and allowing me to explore knowledge, have made me able to carry out this research with pleasure. I will forever remember his heartfelt support and consideration when I suffered mentally and physically.

I am highly grateful to JICA and MEXT for financial aid with medical support, which has made my journey in Japan smoother.

My grateful thanks to the teachers in the Civil Engineering department who, through their lectures, have amazed me with their depth of knowledge and inspired me to aspire for more. I am grateful to East Nippon Expressway Co., Ltd and Mr. Nagata Masashi for providing resources for this research and helping me collect data from the site.

I want to give special thanks to my friends in Japan and Bangladesh, who believed in me, guided me, supported me whenever I needed it, and inspired me during my vulnerable moments.

Lastly, my family, for their love, I am forever grateful.

ABSTRACT

The increase in the length of highways in Japan has led to the excavation of cut slopes through mountains to pave the way for the extension of highways. However, this practice is challenging as mudstone is highly susceptible to weathering. Chemical and physical weathering weaken the cut surface of the slope with time, eventually leading to slope failure. In this study, a mudstone cutslope at Tomei Expressway in Yoshida was studied to investigate the progression of chemical and physical weathering. Results showed that chemical weathering existed before the excavation of the slope in the upper part, while physical weathering occurred after the excavation. Both chemical and physical weathering progressed in the intact nonweathered mudstone in the direction perpendicular to the cut slope surface with time. The upper part of the slope is more chemically weathered compared to the lower part of the slope. Physical weathering was more significant in the lower part of the slope. A novel experiment to accelerate chemical weathering in the laboratory was proposed. The outcome of this test appeared to be useful for instantaneous checks of the chemical weathering state of the mudstone in the field. Moreover, a time-dependent reduction in the strength of the ground was modeled. Finally, the variation of the safety factor and change in the failure mechanism of the slope were investigated. The study provides insights into the formation and progression of weathering phenomena and its effects on the stability of weak rock cut slopes, which is essential for predicting possible slope stability issues and ensuring the safety of highways.

Table of Contents

List of Figures

List of Table

1. INTRODUCTION

The length of highways in Japan is increasing with the necessity of time. Japan is mainly comprised of mountains. Hence, it is bound to have excavated cut slopes through mountains to pave the way for the extension of highways. In many areas, these excavations are carried out through soft sedimentary rocks (UCS of 0.4 – 25 MPa). Therefore, in Japan, a great number of highways have cut slopes in mudstone. A mudstone is a form of sedimentary rock of the Neogene period that alone comprises two-thirds of the sedimentary rock record until now (Schieber, 1999). The associated concern is, mudstone is highly susceptible to weathering. Weathering in a newly exposed mudstone in the environment can start within a few days, weeks, or months (Taylor, 1988). The occurrence of stress release due to excavation results in rehydration and degradation of the mudstone (Hawkins and Pinches, 1992).). Accompanied by slaking, these phenomena lead to the initiation of chemical weathering in the mudstone in the highway cut slope. Physical weathering takes place with time due to the stress release of the cut slope at excavation and mechanical strength reduction. The combined effect of chemical and physical weathering weakens the cut surface of the slope with time, eventually leading to failure. Rapid decomposition can occur in mudstone due to repeated wetting and drying, and they can collapse easily when exposed to water (Okamoto et al., 1981). Due to this fact, engineering works such as excavations through mudstone or sandstone are very challenging as they start to disintegrate at an early stage (Tanimoto, 1982). In recent times, the highway cut slopes are experiencing a long elapse of time after construction and becoming more prone to slope disasters induced by weathering. So, it is very important to study the progress and nature of weathering with time in weak rock cut slopes to predict the possible occurrence of slope stability issues as well as to ensure the safety of the highway. Previously, Pye and Miller, 1990, Chigira and Oyama, 1999, Bhattarai et al., 2007 investigated the weathering of mudstone in the natural mountain and embankment slopes. But no extensive study so far has been conducted for weathering of weak rock cut slopes. To fill the gap, this study aimed to discover the formation and progression of weathering phenomena and their effects on the stability of weak rock cut slopes. Contrasting to a natural slope, excavated cutslope gives a unique opportunity to observe the changes in the soil properties induced by the external environment and internal stress changes from the

beginning of the slope's formation.

In this study, a mudstone cutslope at Tomei Expressway in Yoshida was studied to investigate the progression of chemical and physical weathering. This slope was constructed in 1968 and now has aged more than 50 years after excavation. Seismic wave velocity logging test and elastic wave velocity test have been conducted on this slope periodically throughout 50 years after the construction, which provided a profile of gradual stiffness reduction of the slope with time. A localized collapse occurred on this slope in 2016 due to weathering, which led to a detailed field and laboratory investigation of physical and chemical properties. The primary objective of this study was to discover the extent of weathering and the reduction of the strength of the slope due to weathering by analysing the mineralogy, basic soil properties, strength parameters, and stiffness parameters of the mudstone. A novel experiment was designed and executed on the way to reproduce the field observations regarding chemical weathering of the slope in the laboratory. It aimed to replicate the chemical (pH) and mineralogical changes that occur in the field due to chemical weathering by artificially accelerating the weathering of the mudstone in the laboratory. For this purpose, along with Yoshida, mudstone from another highway cutslope at Zushi was used as the test subject. Combining the results and analysis of the field and laboratory investigations, the time-dependent reduction in the strength of the ground was modelled using the rigid plastic finite element method (RPFEM). Finally, the variation of the Factor of Safety (FS) and change in the failure mechanism of the slope were investigated. A simplified analytical method combining classical slope stability methods was also proposed to capture the variation of the safety factor and change in the failure mechanism of the slope to use instead of RPFEM.

This thesis will be presented in eight chapters. The introduction of the study including the background, objectives, and outline of the research is discussed in Chapter 1. Chapter 2 contains the literature review. Chapter 3 describes the location and geography of the study slope. Field and laboratory tests of Yoshida are stated in Chapter 4. Results and discussions about the field and laboratory test observations are described in Chapter 5. Chapter 5 also includes the details of the accelerated weathering test. Chapter 6 contains the details of the simulation of long-term slope stability. Chapter 7 explains the analytical method for weathered cut slope stability. This study is concluded in Chapter 8 along with the future scope of the study.

2. LITERATURE REVIEW

2.1 Physical and chemical weathering of mudstone

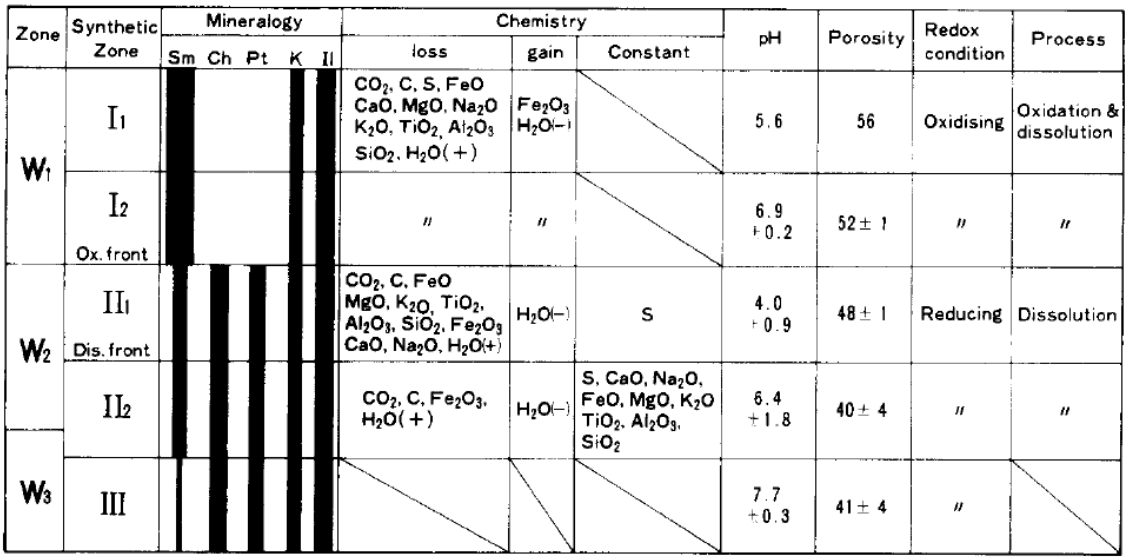

Figure 1 Relationship between weathering zone, mineral composition, chemical composition and physical properties of mudstone (Sm=smectite; Ch=chlorite; Pt=pyrite; K= kaolinite; Il=Illite) (after Chigira, 1990)

Several studies have been conducted in the past to investigate the chemical and physical weathering in mudstone. Mudstone being a soft rock, is sometimes problematic if weathered by causing landslide when this rock is deposited on the surface or interbedded with other soil or rock in the landform (Kojima et al., 2013). Chigira and Kenji, 1987, Chigira M., 1990 and Chigira and Oyama, 1999 conducted studies on the chemical weathering process in natural mudstone slopes located in Japan. From the analysis of the chemical, mineralogical and physical properties of mudstone, they defined the detailed mechanism of chemical weathering in a natural mudstone slope. After a thorough investigation, they divided the process of chemical weathering into different stages based on mineralogical and pH changes termed as weathering zone (Figure 1), which is usually observed in nature. When weathering occurs in a mudstone formation, different weathered zones mentioned in Figure 1 usually form in layers one after another or infused together sometimes. As per their study, weathering in natural mudstone is initiated by the oxidation of pyrite in the oxidized zone by creating an acidic environment. In this zone, the loss of pyrite, calcite and chlorite, along with the increase in smectite mineral, is expected. Due to oxidation of pyrite, natural pH of mudstone changes from alkaline to acidic. Below the oxidized zone,

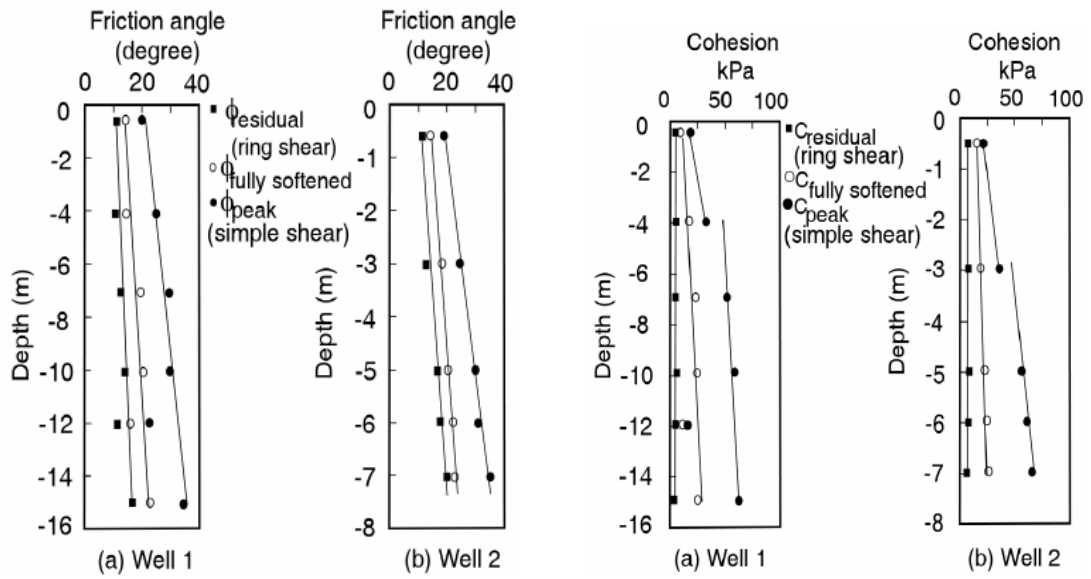

Figure 2 Variation of friction angle and cohesion of mudstone with depth (after Bhattarai et al., 2007)

the dissolution of minerals is continued from the ground water table. Calcite was found to be missing in the weathered mudstone by Hachinohe et al., 1999 indicating dissolution to be one of the reasons that usually occurs during the weathering process (Merrill, 1897). Similar observations were made by Chigira and Sone, 1991 for the case of sandstone mountains in Hokkaido, Japan and by Hayashi et al., 2005 in Horonai mudstone in Japan. Although the mineralogical changes are different in sandstone when compared to mudstone, the similar gradual formation of the weakened weathered zone on the surface of the slope was observed. Pye and Miller, 1990 investigated chemical and biochemical weathering in an embankment made of mudstone. They confirmed the oxidation of pyrite and the development of an acidic environment on the embankment surface. Further, they confirmed the dissolution of carbonate along with the transformation of chlorite into smectite. In an acidic environment created by H_2SO_4 from the oxidization of pyrite, chlorite turns into smectite (Carroll, 1970). Bhattarai et al., 2007 studied the effects of chemical and physical weathering on slope stability in a natural mudstone slope in the Mukohidehara landslide area in Japan. Two important findings from their study are, physical weathering is significant in the groundwater fluctuation zone compared to the rest of the slope, which highly lowers the shear strength in the mudstone slope above the groundwater table. Also, the increase in peak cohesion value is higher than the peak friction angle with depth in the slope (Figure 2). Yoneda et al., 2014 conducted a mineralogical analysis along with slake durability test and

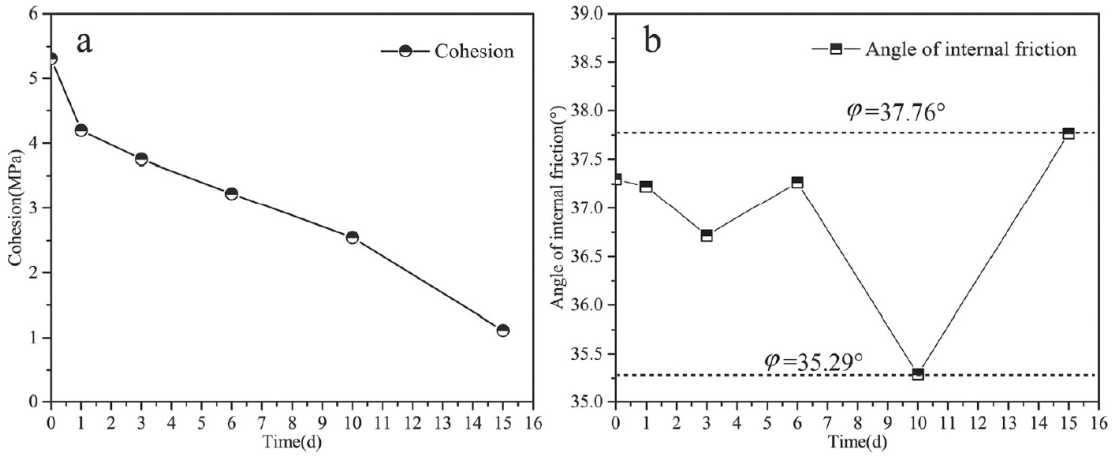

Figure 3 Variation of cohesion and friction angle from dissolution of mudstone by water with time (after Ping et al., 2023)

measurement of the elastic wave velocity of the slaked sample in the mudstone of Central Hokkaido, Japan. They observed oxidation of pyrite and dissolution of chlorite as well in the weathered surface. They concluded that chlorite turns into smectite due to pyrite oxidation, and the abundance of smectite indicates severe weathering in the mudstone.

In humid climates, weathering is primarily caused by water and oxidation of the minerals present in the mudstone (Carroll, 1970). Repeated wetting and drying action above the water table leads to the oxidation process which induces weathering in the mudstone. Emerson, 1964; Pusch, 1983; Ruiz-Vera and Wu, 2006 showed that clay minerals contribute to the process of slaking that has a direct influence on physical weathering. Besides slaking, changes in the daily and seasonal temperature, pore water freeze-thaw action and changes in the relative humidity also have significant effects on physical weathering in the unsaturated zone above the water table in a mudstone slope (Wetzel and Einsele, 1991; Price, 2013).

The usual colour of natural intact mudstone is dark grey or black (Hawkins & Pinches, 1992; Cull, 2009). On the occurrence of weathering, there is a distinct change in colour from dark grey to brownish grey (Koma et al., 1983; Hawkins & Pinches, 1992; Oyama & Chigira, 2000). Above mentioned research has proved that, along with changes in appearance, mineralogical changes also take place in the mudstone when weathering occurs. Hence, weathering in mudstone is indicated primarily by the changes in colour from dark grey to brown, changes in pH from alkaline to acidic, increment of

smectite and simultaneous disappearance or loss of pyrite and chlorite. Confirmation of these mineralogical changes could be found in Warren and Lynn, 1966; Russell and Parker, 1979; Senkayi et al., 1981; Dixon et al., 1982; Chigira and Oyama, 1999; Chigira M., 1990; Pye and Miller, 1990; Bhattarai et al., 2007; Susan et al.,2013; Yoneda et al., 2014.

Bhattarai et al., 2007 concluded that physical weathering has a significant effect on the reduction of peak shear strength. Stress release due to the excavation of mudstone plays a key role in the physical weathering of mudstone (Cripps and Czerewko, 2017). Tran et al., 2012 and Ciantia et al., 2015 observed that strength reduction due to the physical weathering of soft rocks is led by the dissolution of soluble minerals as well.

However, physical and chemical weathering in soft rocks such as mudstone progresses simultaneously (Matsumoto et al., 2017). Knopp et al., 2022 showed that, mineral leaching due to chemical weathering increases the porosity of the soft rocks, which directly influences the strength of the material by reducing its density. Again, repeated wetting and drying above the groundwater table increases the rate of chemical weathering and the progression of it into the deeper parts of the slope from the surface. Hence, both chemical and physical weathering directly influence each other and these two phenomena should be discussed together.

2.2 Experiments on physical and chemical weathering of soft rocks in the laboratory

Both internal and external environmental factors affect weathering of the mudstone, which leads to the decrease of the strength and the stiffness leading to degradation. Research has been done previously to check the process of physical and chemical weathering of soft rock and the variation of physical and chemical properties with weathering. Chigira, 1993, in the laboratory, recreated the weathered zones that are naturally found in the mudstone at a small scale. He developed oxidation and dissolution fronts in intact mudstone samples by putting them under axial stress in a pH and DO-controlled bath. He also confirmed the depletion of pyrite, calcite, and chlorite and the development of smectite. In his experiment, he observed increased porosity, decreased density, P-wave velocity and shear strength as weathering progressed in the mudstone. Lu et al., 2016 showed with uniaxial test and

X-ray CT of mudstone in a temperature-controlled and water-submerged environment the effect of the water and temperature in the degradation of mudstone. Ping et al., 2023 checked the dissolution of mudstone in distilled water and showed that the porosity increased and cohesion decreased with time with little variation in the angle of friction (Figure 3). Marty et al., 2018 conducted a flow-through experiment on claystone in atmospheric conditions and checked the leaching rate of minerals. Ciantia et al., 2013 checked disintegration characteristics and developed a model of weathering of calcarenite (a type of soft rock). Pye and Miller, 1990 weathered mud rock in the laboratory with diluted (0.14%) sulfuric acid (pH 1.8) and checked the mineralogical variation with time. Weisener and Weber, 2010 checked the rate of pyrite oxidation in the laboratory by putting mudstone in a humid chamber. They checked the difference in reactivity between two different forms of pyrite. Sutton et al., 2013 did a detailed experiment to discover the swelling properties of the mudstone by submerging mudstone samples in mineral water of 7.2 ± 0.1 pH. In this experiment, the variation of pH with time was checked along with the oxidation of pyrite. Ning et al., 2003 evaluated the mechanical properties of sandstone under acid solutions. Rock samples were submerged in an acid solution of pH 1, 3, 5, and 7. Uniaxial compression test (loading rate 0.5 MPa/s) and X-ray CT was performed in the samples after 5, 9, 14, and 21 days. They observed that the uniaxial compressive strength of the samples reduced with the reduction in pH and increase in the submerged period.

Several experiments have been done in the past to weather soft rock using the salt solution and observe the degradation due to salt weathering (Goudie, 1986, Lee and Yoon, 2017, Sperling and Cooke, 1985). However, no direct laboratory experiment was found that captured the accelerated weathering process using an acidic environment and analysed the changes in pH and mineralogy caused by chemical weathering in mudstone.

2.3 Simulation of soft rock slope stability influenced by weathering

Vlastelica and Miščević, 2012 checked the stability of an excavated marl slope with weathered joints by varying cohesion while keeping the angle of friction value at 30°. They evaluated the possibility of slope failure by sliding of the existing joints in the slope.

Singh et al., 2008 investigated the physical properties of different rock cut slopes situated in the northern part of India and used those as parameters for the analysis of the stability of the slopes to predict landslides with a finite difference model. Zheng et al., 2017 conducted a simulation to observe displacement distribution and factor of safety using the distinct-element method in a sandstone and mudstone interbedded slope and tried to understand the slope failure mechanism. The effect of softening in the mudstone slope stability was analysed by Yoshida et al., 1991 using the elastoplastic finite element method. Utili and Crosta, 2011 performed a detailed limit analysis to evaluate the stability of weathered rock slopes.

A detailed study on the combination of chemical and physical weathering in excavated mudstone cutslope is not considered yet. Moreover, a clear discussion on the weathering induced reduction of strength and stiffness affecting the stability of the cutslope is missing.

3. TARGET SLOPES LOCATION AND GEOGRAPHY

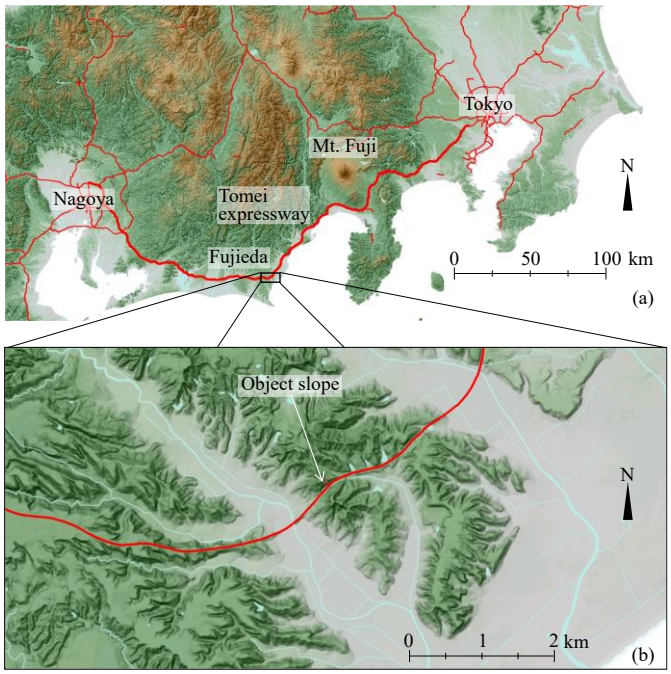

Figure 4 Location map of the cut slope at Yoshida

The study area for this research consists of two highway slopes. One is a cut slope of Tomei Expressway situated at Yoshida town in Shizuoka prefecture, Japan (Figure 4). The hill through which the cut slope was excavated was originally formed in the Neogene period (Figure 5). Figure 6 shows the different states of the slope after excavation at different times. Vegetation on the slope surface was cleared periodically. A front view of the slope, along with the field test locations and boreholes, is shown in Figure 7. The slope is mainly composed of uniform mudstone with intermittent layers of sandstone which is roughly depicted in the cross-section of the slope in Figure 8. Thin sandstone layers are also embedded in some parts of the formation. In this slope, the soil formation layers are almost perpendicular to the slope surface. At the top of the formation, the soil layer was composed of alluvial soil deposited in the quaternary period. This top layer was completely removed during the excavation of the cut slope as the layer was very weak in strength.

Another slope is situated in Zushi, Kanagawa. Figure 9 shows the geological formation of the slope. This slope mainly consists of mudstone like Yoshida with intermittent sandstone layers. The soft rock layer formation in this slope is parallel with the cut slope surface. The top layer of the slope was completely removed by a landslide occurring from heavy rain in 2022.

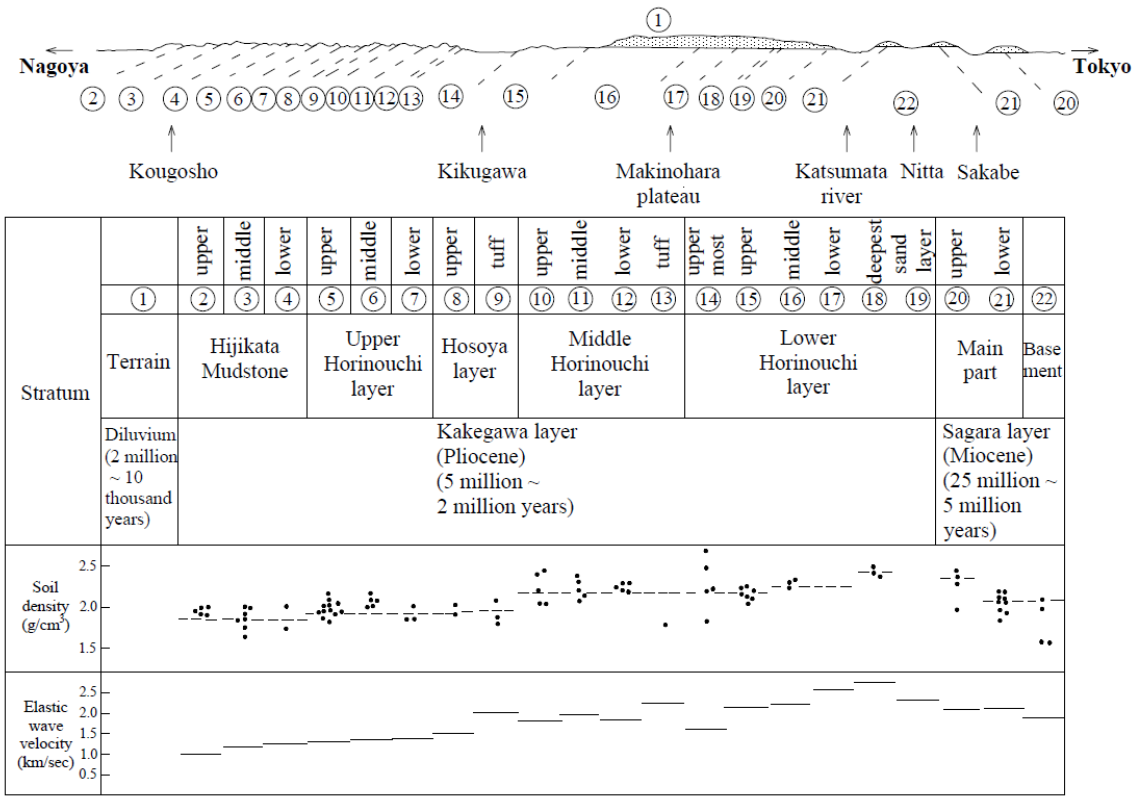

Figure 5 Geology along Tomei expressway around Makinohara Neogene layer (after Inada et. al.)

1971 (after 3 years of excavation)

2001 (after 33 years of excavation)

1985 (after 17 years of excavation)

2017 (after 49 years of excavation)

Figure 6 Picture of the cut slope at Yoshida taken at different times

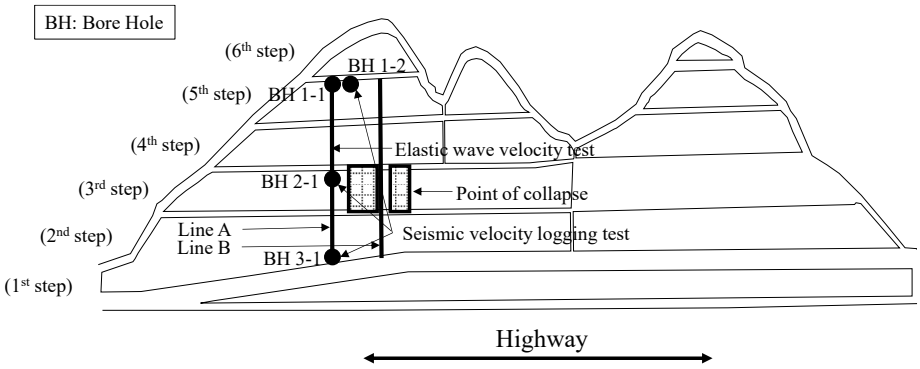

Figure 7 Front view of the cut slope with borings and testing locations

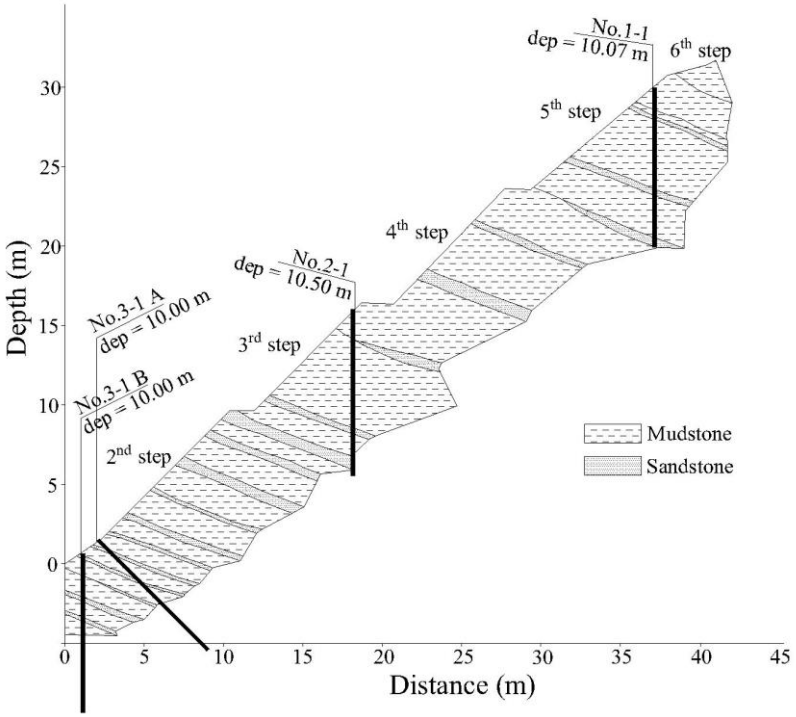

Figure 8 Cross section of the slope at Yoshida with geological description (along line A)

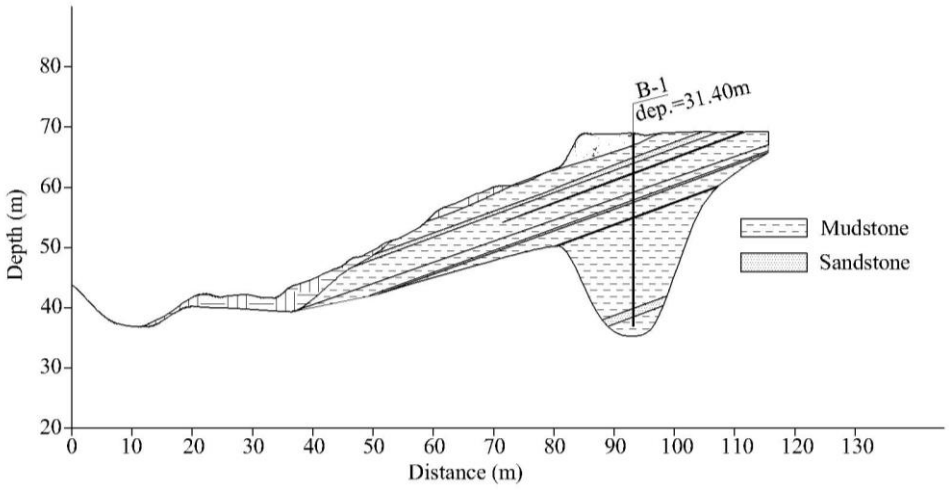

Figure 9 Cross section of the slope at Zushi with geological description

4. FIELD AND LABORATORY TESTS OF YOSHIDA

4.1 Field tests of Yoshida

Various field tests were conducted to obtain different soil parameters of the cut slope for the analysis, which are described in this section.

4.1.1 Soil boring and sampling

Soil sample collection and subsurface exploration were done using five boreholes dug up to 10.0-10.5 m from the surface. Soil samples were also collected from the surface of the cut slope to check different soil properties. The positions of the boreholes are shown in Figure 7 and Figure 8. BH (borehole) 1-1 and 1-2 are situated within 1.0 m of each other and are located at the upper part of the cut slope. BH 2-1 is located at the middle part of the cut slope, and at the bottom of the cut slope, BH 3-1 A and BH 3-1 B are positioned. Soil samples collected from BH 1-1, 1-2, 2-1, and 3-1 B were used for laboratory testing. BH 3-1 A was used as a survey hole to conduct a periodical geophysical survey starting from the construction of the slope.

4.1.2 SPT (Standard Penetration Test)

In borehole 1-1, SPT was conducted, and at an interval of every 0.5 m, SPT N value and soil samples were collected to evaluate the geotechnical properties of soil. In boreholes 2-1 and 3-1 B, SPT was not conducted. Only soil samples were collected at an interval of 0.5 m. From visual inspection and the colour of the samples, soil type and extent of weathering were determined for each sample in boreholes 1-1 and 2-1.

4.1.3 Seismic and density logging

Seismic velocity logging was conducted along line A and line B (Figure 7) according to JGS 1122-2012 (downhole method) to evaluate the stiffness of the mudstone in the cut slope. BH 1-2, 2-1 and 3-1 A fall along line A. From this test, the velocity of the elastic waves (P-wave and S-wave) travelling in the ground was obtained. Elastic wave velocities were used to obtain the shear modulus, Poisson's ratio and Young's modulus of the mudstone along the boreholes. In 2017, this test was conducted in BH 1-2 and 2-1, but in borehole 3-1 A, this test was conducted in the years 1971, 1978,

1985 and 2017. Density logging was done in the field along BH 1-2 and 2-1 using a nuclear gauge by following the method of JGS 1614-2012. The in-situ density of the soil samples was also obtained using radioactive isotopes.

4.1.4 Elastic wave exploration test

Subsurface ground conditions along the cut slope were investigated by elastic wave exploration in the years 1971, 1978, 1985 and 2017 using the seismic refraction method. The stiffness of the mudstone at different depths was obtained from the data of the elastic wave velocities found at different depths. Along lines A and B (Figure 7), 23 geophones were positioned at 1.5 m intervals along each line to collect the refracted wave originating from a fixed source point. Distribution of stiffness in the slope was obtained by producing seismic waves with a hammer at the source point, receiving refracted waves by the geophones and interpreting the output as P and S wave velocity from the seismograph. The subsurface condition was imaged by the layer-stripping method from tests conducted in 1971, 1978, 1985 and 2017. From this, along lines A and B, the profile of the changes in the velocities of the P and S waves was depicted. In 2017, seismic tomography was used to interpret the 2D colour contour map of the subsurface condition showing different velocities of P and S waves at different depths, thus providing a clearer image of the gradual reduction of stiffness of the slope with time.

4.2 Laboratory test of Yoshida

Several laboratory tests were conducted using the soil samples collected from the boreholes and the slope surface to investigate the weathering of the mudstone cut slope. Methods of these tests are described below:

4.2.1 Mineralogy

Powder XRD (X-Ray Diffraction) analysis was conducted to discover the mineralogical composition of the mudstone. Samples collected from BH 1-1, BH 2-1 and the surface of the 4^{th}, 5^{th} and 6^{th} steps of the slope were checked initially. Intensity graphs of the samples are presented in Figure 10 - Figure 14. In the boreholes, samples were marked in the depth direction starting from the top of the borehole. The samples collected from the surface along the slope are marked according to the measured distance in the downward direction starting from the top of each corresponding step. For this

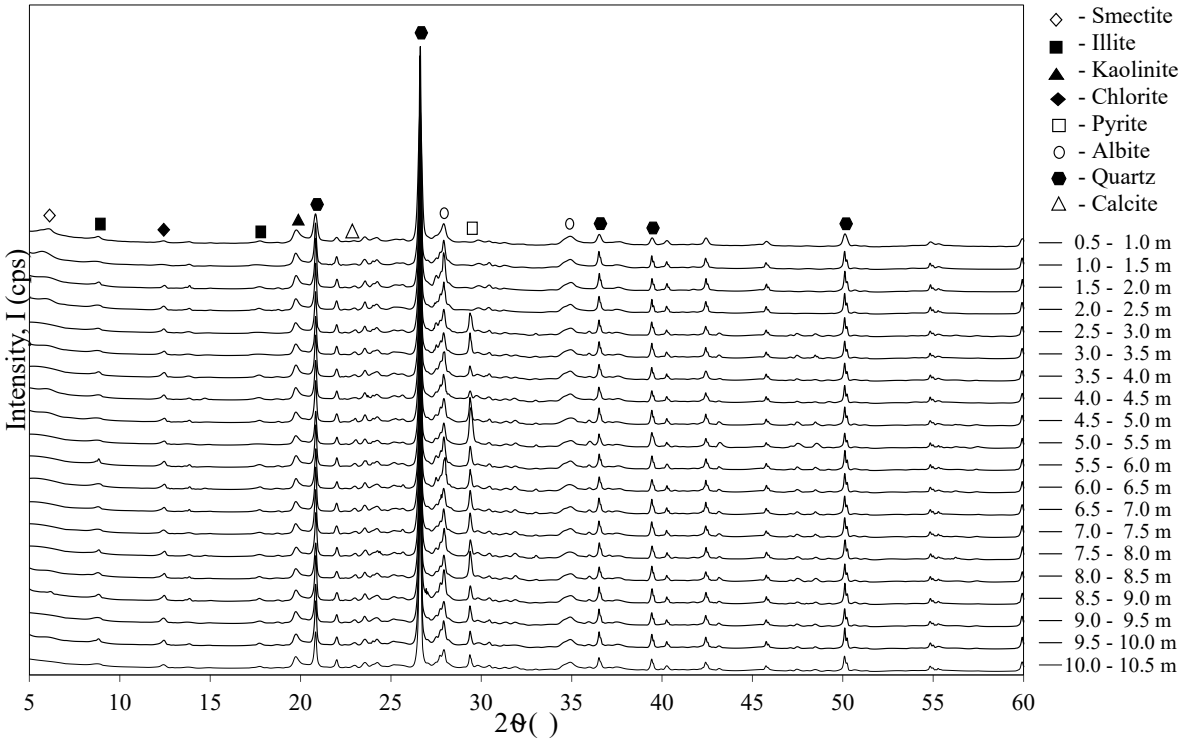

Figure 10 XRD graph of BH 1-1

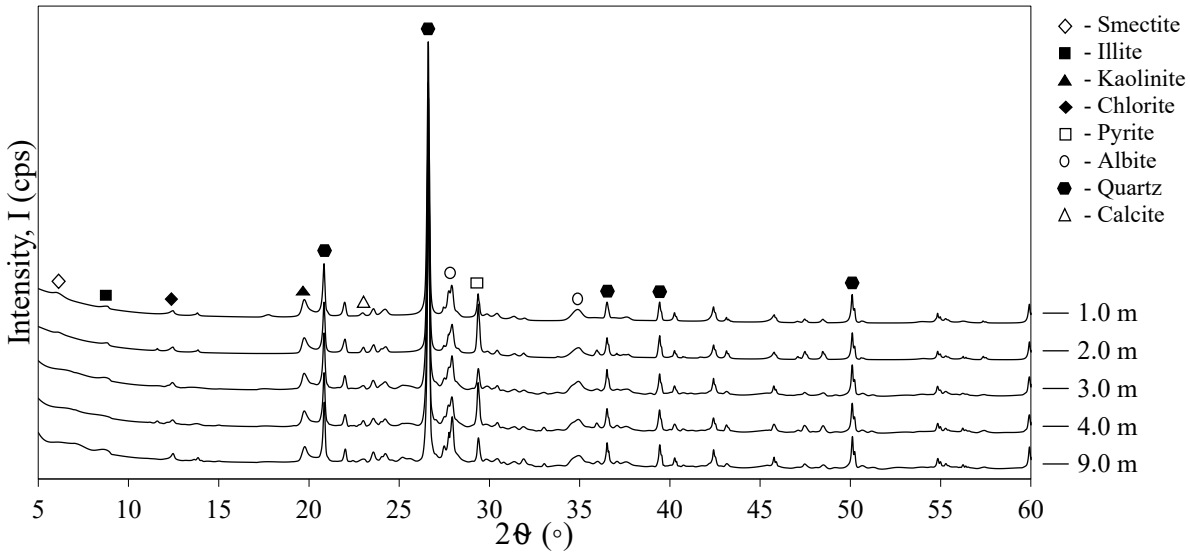

Figure 11 XRD graph of BH 2-1

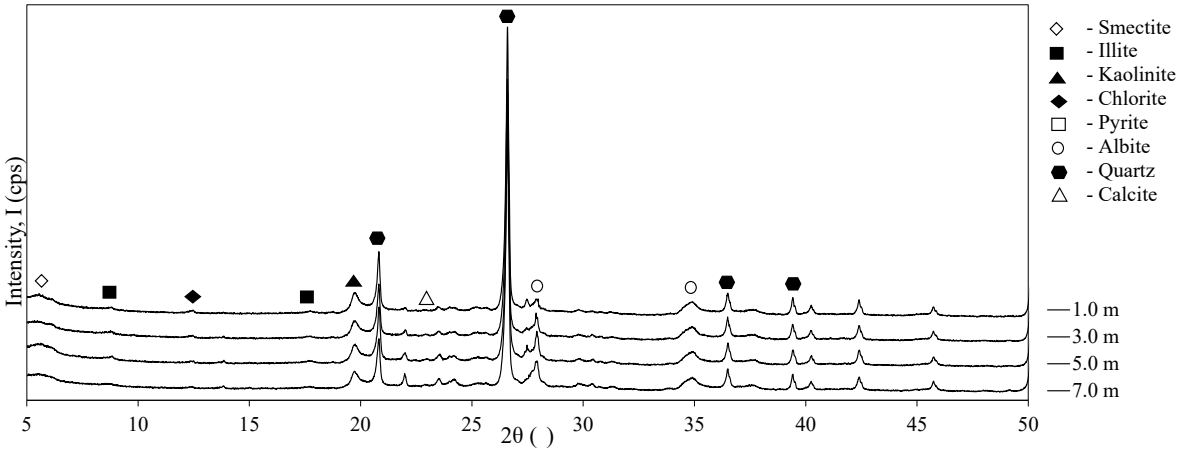

Figure 12 XRD graph of the 6th step

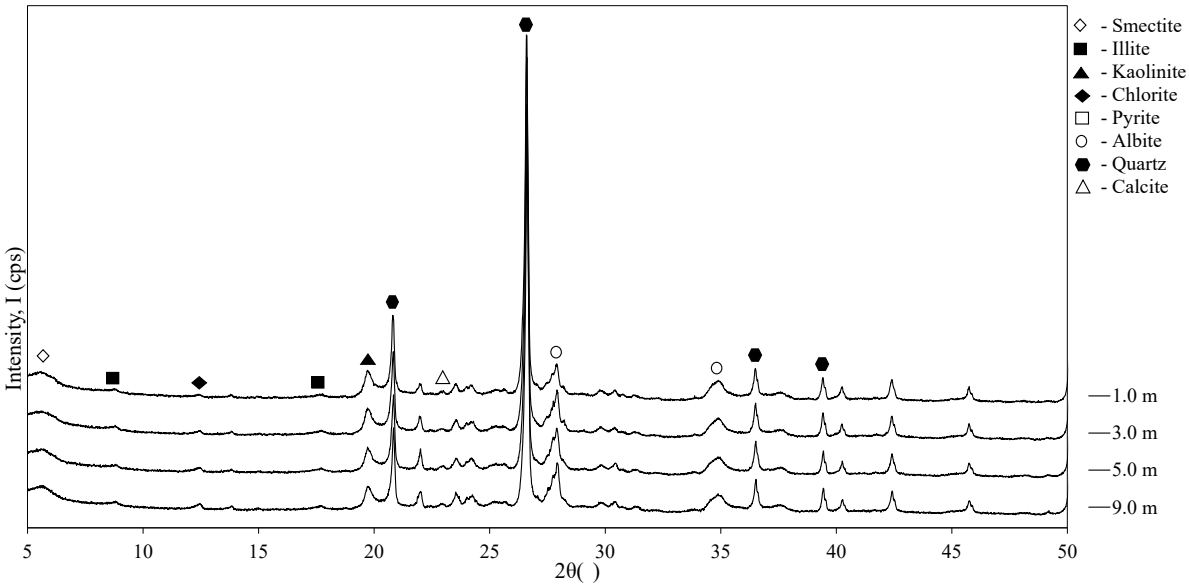

Figure 13 XRD graph of the 5th step

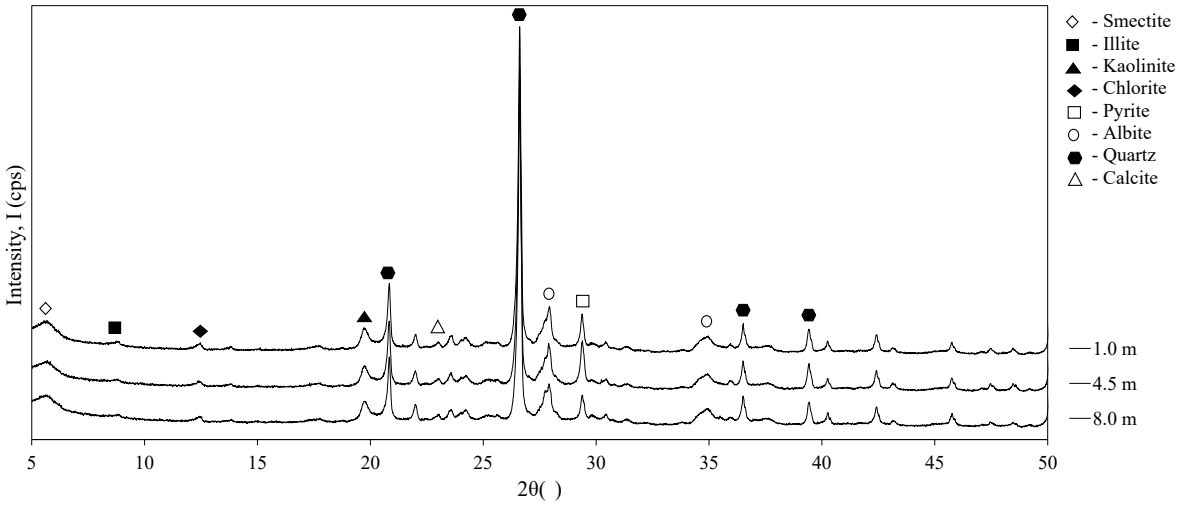

Figure 14 XRD graph of the 4th step

test, soil samples collected from the site were initially oven-dried at 40° C for 24 hours. The oven-dried samples were ground into a powder and sieved through a 53μm sieve afterwards. Sample glass plates were prepared with the powder sample for analysing in the diffractometer. Rigaku SmartLab X-ray diffractometer was used to obtain 2D powder diffraction patterns Figure 10 - Figure 14. For the identification of minerals present in the samples, methods described by Ulrey and Drees, 2008 and Moore Reynolds Jr., 1989 were followed. XRD intensity peaks generated from d-spacings (the spacings between atomic planes of the concerned minerals parallel to their dominant cleavage face) were used to detect the presence or absence of minerals. d spacing in the mineral crystals is formed in the 3-D space with different h, k, l (miller indices) values and diffraction angles unique to each mineral. Hence the reflections from the mineral crystals are labelled as dhkl (Å), which is prime information needed for the identification of the minerals. First-order basal reflections of minerals, which are d00l (Å), were obtained for each diffraction pattern from Rigaku SmartLab Studio II software after the completion of the analysis in the diffractometer. The reflection provided by d00l plane of the clay minerals is usually most intense and very helpful in recognising the mineral from the intensity graph. The general procedure followed for the identification of minerals was searching for minerals associated with strong peaks of diffractogram and confirming the mineral by finding the position of its weaker peaks at 2θ ( ) from the d-spacings. By repeating the process, minerals present in the samples were identified.

For the relative quantification of minerals, after baseline correction of the diffractogram, the height of the peak for each mineral was measured. For all samples, the height was checked, and the maximum height for each mineral in the soil samples from BH 1-1 was identified. The relative quantity of the minerals was obtained by dividing the height of the peak of the mineral present in each sample with the maximum height of the same mineral found in BH 1-1 and multiplying it by 100. It can be formulated as:

$$I_r = \frac{I}{I_{max}} \text{ x } 100\ \% \quad (1)$$

Where,

I_r = Relative intensity of the mineral among all the samples of a borehole

I = Actual intensity of the mineral in the associated sample

I_{max} = Maximum intensity of the mineral found in samples of BH 1-1

4.2.2 Physical properties

In the laboratory, following the method described in JGS 0211-2009, a pH test was conducted with the soil samples collected from BH 1-1, 2-1 and the surface of the slope. The moisture content of the soil samples collected from BH 1-2 and 2-1 was obtained by JIS A 1203:2009. The dry and wet density of soil samples collected from BH 1-2 and 2-1 were determined in the laboratory according to JGS 0191/JIS A 1225.

4.2.3 Strength parameters

Needle penetration test and Uniaxial loading test were conducted with the samples collected from BH 1-2 and 2-1 at different depths to get the strength parameters of the mudstone of the slope. Results of the needle penetration test were converted in unconfined compressive strength (UCS) from NPR (needle penetration readings) using the correlation introduced by the needle penetrometer SH-70 manufacturer [Maruto corporation, 2006]:

$$\log \mathrm{UCS} = 0.978 \log \mathrm{NPR} + 2.621 \quad (2)$$

Here, UCS is expressed in kN/m^2 and NPR in N/mm.

5. WEATHERING MECHANISM AND PROGRESS IN CUT SLOPES

5.1 Variation in mechanical properties of the cut slope at Yoshida

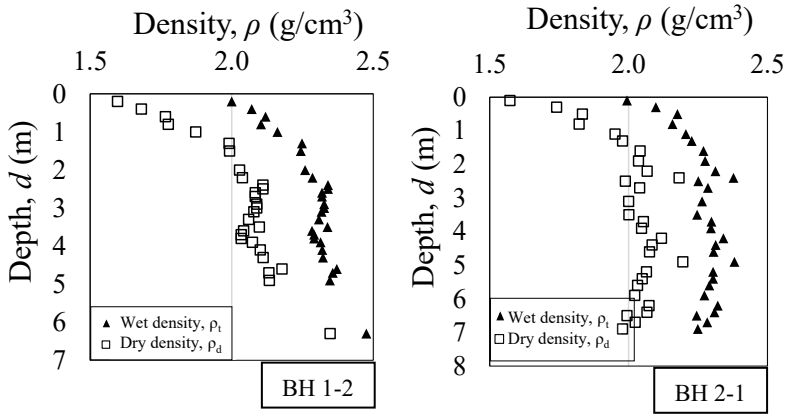

Figure 15 Summary of the results of mudstone density

Table 1 Seismic velocity logging results of BH 1-2

Depth of soil layer (m)	V_p (m/s)	V_s (m/s)	Poisson's ratio, ν	Shear modulus G (MPa)	Young's modulus E (MPa)
0.00 - 1.00	340	190	0.273	0.071	0.181
1.00 - 1.35	410	220	0.298	0.103	0.267
1.35 - 1.75	410	220	0.298	0.106	0.275
1.75 - 2.00	410	220	0.298	0.109	0.283
2.00 - 3.50	680	270	0.406	0.165	0.464
3.50 - 5.00	1070	440	0.398	0.441	1.230
5.00 - 7.00	1320	550	0.395	0.716	2.000
7.00 - 10.00	2050	550	0.461	0.722	2.110

Evaluation of physical weathering was carried out from the analysis of rock density, seismic logging, and elastic wave exploration test results at Yoshida. The density of the mudstone along the BH 1-2 and 2-1 was obtained from density logging at the site as well as laboratory testing. The results are presented in Figure 15. Results of density logging gave similar trends as wet density obtained for the samples of the same depth from laboratory tests validating the results of density logging. From the results, it can be conceived that the density of the mudstone tends to be lower in the upper part of the boreholes due to physical weathering, while it is denser in the deeper part.

Table 2 Seismic velocity logging results of BH 2-1

Depth of soil layer (m)	V_p (m/s)	V_s (m/s)	Poisson's ratio, ν	Shear modulus G (MPa)	Young's modulus E (MPa)
0.00 - 1.00	340	190	0.273	0.073	0.187
1.00 - 2.00	460	250	0.290	0.137	0.354
2.00 - 3.50	1010	250	0.467	0.141	0.414
3.50 - 4.50	1380	400	0.454	0.362	1.050
4.50 - 8.00	1780	440	0.467	0.436	1.280
8.00 - 10.90	2050	650	0.444	0.957	2.760

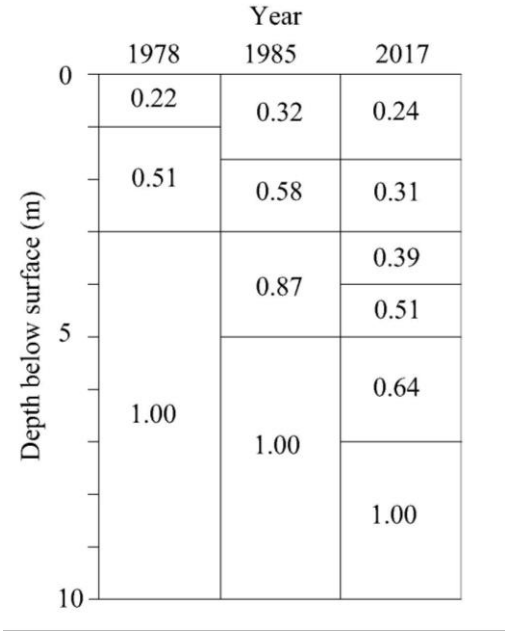

Figure 16 Composition of normalized Seismic velocity logging (p-wave) test results of BH 3-1

The shear modulus of the upper and lower part of the slope obtained from seismic velocity logging represents the variation in stiffness in the surficial and deeper part of the cut slope. Results of seismic logging conducted at BH 1-2 and 2-1 are given in Table 1 and Table 2. In both boreholes, due to physical weathering and stress release from the excavation, the stiffness of the intact mudstone was reduced significantly in the surficial part, especially above 3.5 m. Figure 16 is the plot of the normalized P-wave velocity (V_p) obtained by seismic logging in BH 3-1 in the years 1978, 1985 and 2017. This figure depicts the reduction in stiffness in the perpendicular direction of the slope surface in 50 years. The elastic wave exploration test also revealed the weathered condition of the soil. Figure 17 and Figure 18 show the contour map of the seismic velocities found from the test conducted by layer - stripping

method in the year 2017. Along lines A and B, seismic velocities were found to be low in the surficial region of the cut slope, but in the perpendicular direction of the cut surface, the velocities increased in the deeper part of the mudstone deposit. A tomographic map of elastic wave exploration conducted in the same year and in the same area is presented in Figure 19 and Figure 20. These colour contour maps show a clear and gradual increase of wave velocities from the surface to the deeper part of the slope in a perpendicular direction along lines A and B. Evaluating the variation of elastic waves, it was found that, within 50 years, up to the depth of 3.0 m from the surface, stiffness reduced to one-third of its original strength due to physical weathering.

The strength of the mudstone of the cut slope was revealed by obtaining q_u (UCS) parameter by combining the uniaxial loading test and needle penetration test. Figure 21 is the plot of depth vs UCS of BH 1-2 and 2-1. From this test, it could be interpreted that the strength of the intact mudstone is around 4000-3000 kN/m^2. But above 3.0 m in both boreholes, the strength reduced and became approximately 2000 kN/m^2. Initially, before, and right after the excavation of the slope, the whole cut slope can be expected to have a uniform strength. This reduction in strength in the depth of around 3.0 m occurred within 50 years. The reduced strength is an indicator of the occurrence of physical weathering in the concerned slope.

The overall tendency observed in the mechanical properties of the mudstone cut slope is the reduction in density, stiffness, and strength in the surficial part along the cut slope compared to the intact mudstone in the deeper part. A gradual and significant decrease in the stiffness and strength of the slope was detected, which took place within 50 years after excavation. This overall tendency marks the progression of physical weathering in the intact mudstone starting from its surface.

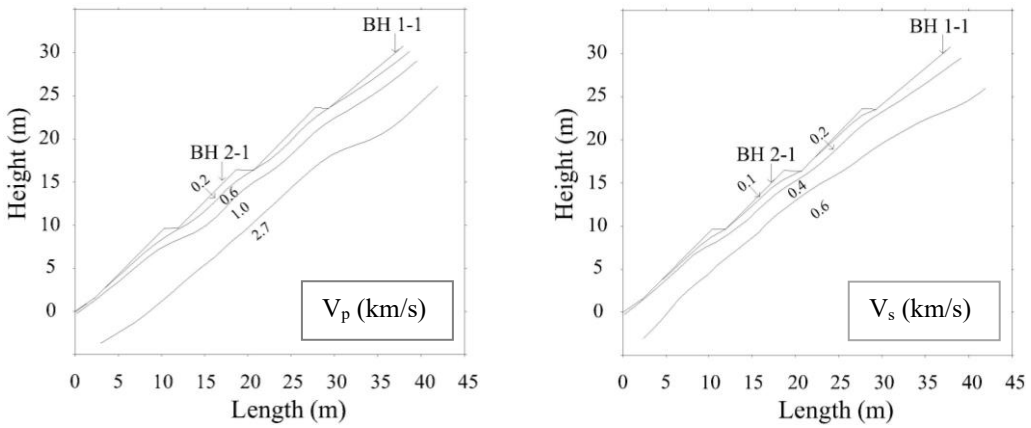

Figure 17 Contour map of Elastic Wave Exploration along line A (layer-stripping method)

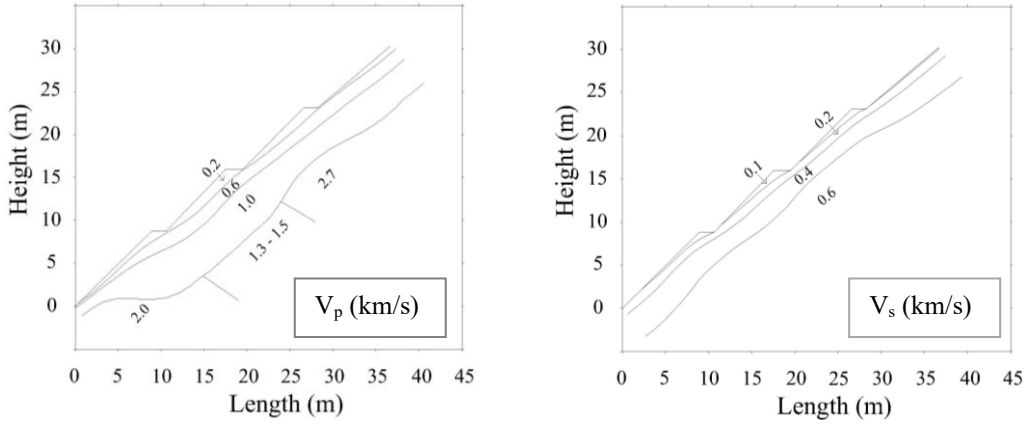

Figure 18 Contour map of Elastic Wave Exploration along line B (layer-stripping method)

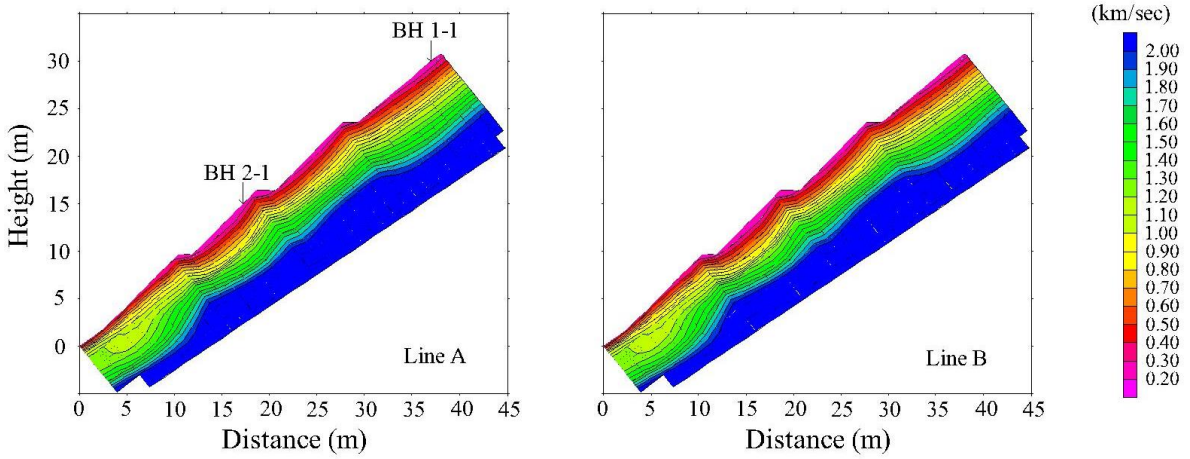

Figure 19 Contour map of Elastic Wave Exploration (V_p) (Tomography)

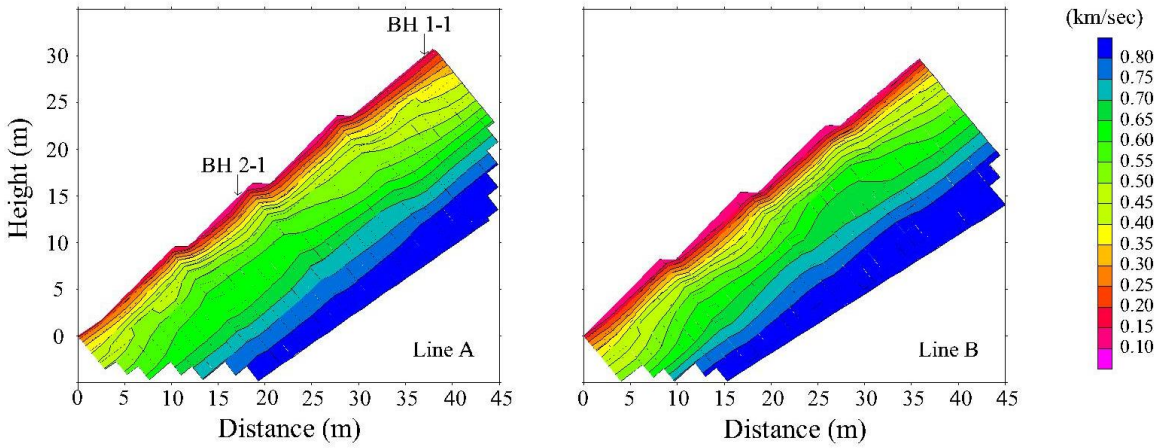

Figure 20 Contour map of Elastic Wave Exploration (V_s) (Tomography)

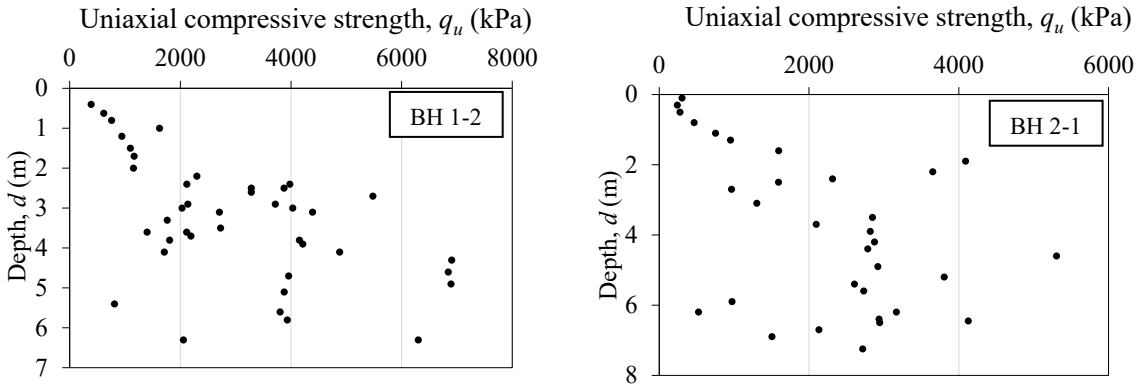

Figure 21 Results of unconfined compressive strength (UCS) of the slope

5.2 State of chemical weathering at the cut slope at Yoshida

Geophysical prospecting of the study area was conducted through soil boring. Table 3 and Table 4 present the information obtained about soil strata from mudstone samples of BH 1-1 and 2-1. Uniform mudstone was found in the slope with intermittent layers of sandstone. The water table was found at 2.0 m and 3.05 m, respectively. From visual inspection, until about 4.0 m depth of both boreholes, mudstone was identified to be weathered while intact mudstone was observed below that depth. The colour of the mudstone in the detected weathered zone was brownish-grey. In the intact areas or the deeper part of the borehole, the colour was dark grey. A distinct change in the colour from dark grey to brownish-grey ensured the presence of weathering along the surficial part of the cut slope to a significant depth. SPT N value was low in the surficial part of BH 1-1, which was identified as a strongly weathered zone compared to the intact mudstone.

Table 3 Soil properties along BH 1-1

Depth of soil layer (m)	Colour	Type of the soil	State of the soil	SPT N
0.5 - 1.0	Brownish grey (Light)	Mudstone	Strongly weathered	21
1.0 - 1.5	Brownish grey (Light)	Mudstone	Strongly weathered	38
1.5 - 2.0	Brownish grey (Light)	Mudstone/sandstone	Weathered	50
2.0 - 2.5	Brownish grey	Mudstone	Weakly Weathered	50
2.5 - 3.0	Brownish grey	Mudstone	Weakly weathered	50
3.0 - 3.5	Dark grey	Mudstone	Weakly weathered	50
3.5 - 4.0	Dark grey	Mudstone	Weakly weathered	50
4.0 - 10.5	Dark grey	Mudstone	Intact	50

Table 4 Soil properties along BH 2-1

Depth of soil layer (m)	Colour	Type of the soil	State of the soil
0.00 - 1.00	Brownish dark grey	Mudstone	Weathered
1.00 - 2.00	Brownish dark grey	Mudstone	Weathered
2.00 - 4.50	Dark grey	Mudstone	Weakly weathered
4.50 - 10.50	Dark grey	Mudstone	Intact

Mineralogical analysis of the samples of boreholes and the surface of the slope done from intensity graphs are presented in Table 5, Table 6, and Table 7, respectively. Following the procedure of the quantification of the minerals described in Chapter 4.2.1, when the basal reflection of a specific mineral was not detected in a sample, the mineral was considered absent in that sample, and the quantity of that mineral in that sample was denoted as “None” in Table 5, Table 6, and Table 7, and no colour was assigned for its quantification. Depending on the value of I_r for each mineral, the light grey colour was assigned to those samples where the presence of the mineral was found to be low, such as greater than 0% to lower or equal to 40% compared to the I_{max} for that specific mineral. The dark grey colour was assigned where the value of I_r was found to be moderate, greater than 40% to lower or equal to 70%. An abundance of the mineral was marked by the presence of more the 70% to 100% mineral, and black colour was assigned in this quantification. Table 5 and Table 6 include the pH of the samples as well. Quartz and mica were the main constituting mineral of the concern slope, and their content was found to be consistent in both boreholes. Among all the minerals found, only the relative quantities of clay minerals are presented in the tables. Illite and kaolinite content varied along BH 1-1, but in the rest of the areas, their amounts were stable. Other minerals found in the samples were:

Table 5 Summary table of the results of XRD analysis and pH test of BH 1-1

Depth(m)	Color	Zone	Fronts	Mineralogy	pH	q_u (kN/m^2)
0.5	Brownish gray (Light)	W1	Oxidized zone			
1.0						
1.5						
2.0	Brownish gray		Oxidation			
2.5						
3.0		W2	Front			
3.5						
4.0						
4.5						
5.0	Dark gray	W3	Zone of dissolution and fresh rock			
5.5						
6.0						
6.5						
7.0						
7.5						
8.0						
8.5						
9.0						
9.5						
10.0						
10.5						

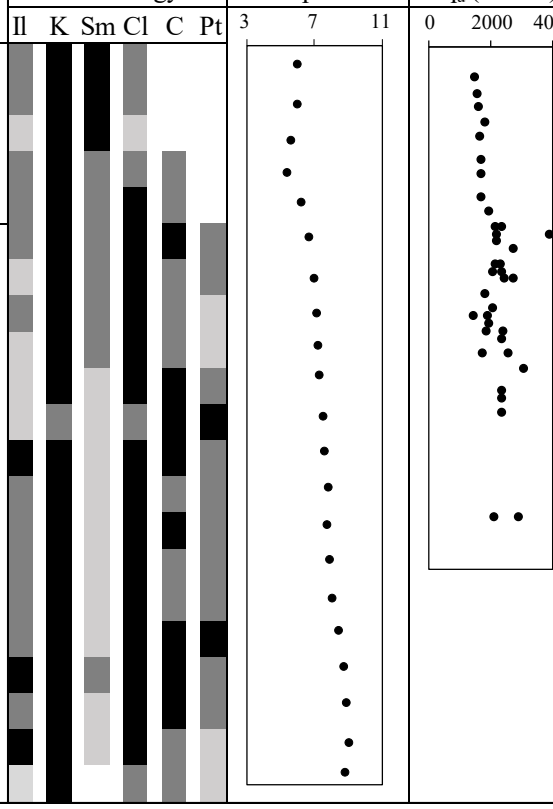

W1 - heavily weathered
W2 - moderately weathered
W3 - weakly weathered/fresh rock

Il – Illite
K – Kaolinite
Sm – Smectite
Cl – Chlorite
C – Calcite
Pt – Pyrite

70 - 100 %
40 - 70 %
0 - 40 %
None

Table 6 Summary table of the results of XRD analysis and pH test of BH 2-1

Depth (m)	Color	Zone	Fronts	Mineralogy	pH	q_u (kN/m^2)
1.0	Brownish dark gray	W3	Zone of dissolution and fresh rock			
2.0						
3.0	Dark gray					
4.0						
5.0						
6.0						
7.0						
8.0						
9.0						

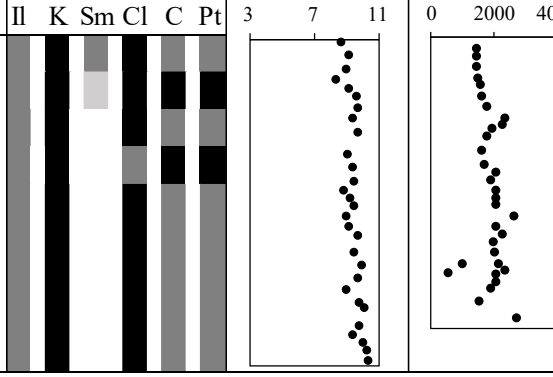

W1 - heavily weathered
W2 - moderately weathered
W3 - weakly weathered/fresh rock

Il – Illite
K – Kaolinite
Sm – Smectite
Cl – Chlorite
C – Calcite
Pt – Pyrite

70 - 100 %
40 - 70 %
0 - 40 %
None

Table 7 Summary table of the results of XRD analysis of the samples collected from the slope surface

Boring area	Sample No. (Downward from top at 1.0 m interval)	Mineralogy					
		Il	K	Sm	Cl	C	Pt
BH 1-1	1						
	2						
	3						
	4						
	5						
	6						
	7						
	8						
BH 2-1	1						
	2						
	3						
	4						
	5						
	6						
	7						

Il – Illite
K – Kaolinite
Sm – Smectite
Cl – Chlorite
C – Calcite
Pt – Pyrite

70 - 100 %
40 - 70 %
0 - 40 %
None

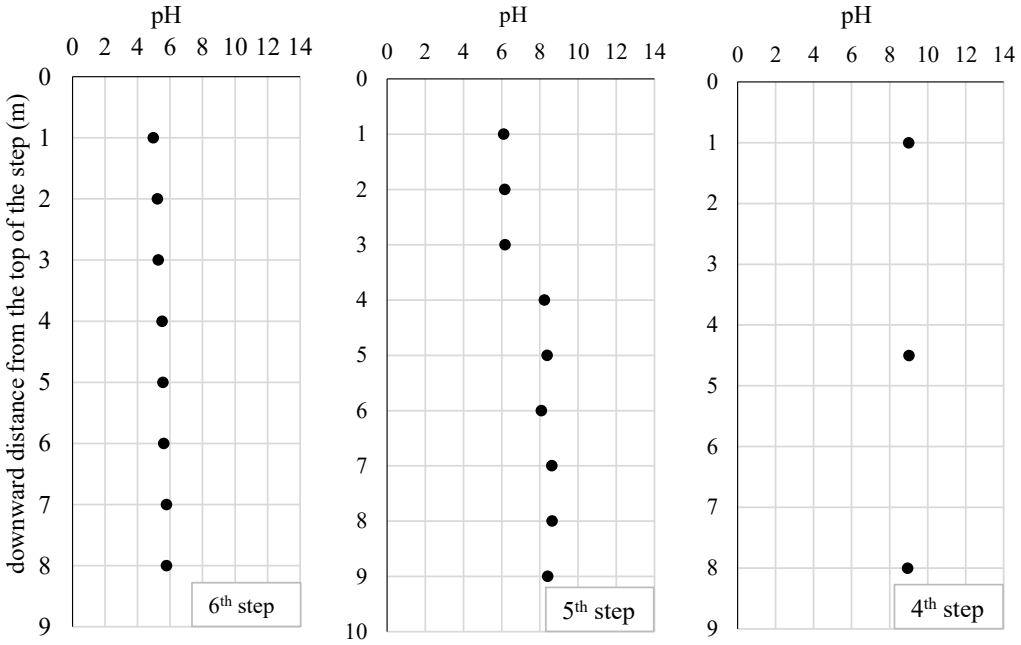

Figure 22 Variation in pH in the samples collected from the surface of the slope

Smectite, Chlorite, Calcite, and Pyrite. In BH 1-1 (Table 5), above around 3.0 m, compared with the deeper part of the borehole, smectite content became abundant, chlorite content decreased, and calcite and pyrite disappeared. On the other hand, in BH 2-1 (Table 6), above 3.0 m, smectite was detected while it was absent below that depth. In this borehole, some reduction of calcite and pyrite was marked in the surficial area. On the surface (Table 7), smectite was abundant in all parts of the slope. A decrease in chlorite content and the missing calcite and pyrite content was observed in the upper part of the slope in comparison with the lower part. pH value of BH 1-1 (Table 5) indicated an acidic environment above 3.0 m, and below that, pH was alkaline. In BH 2-1 (Table 6), pH was alkaline throughout all the depths of the borehole. Figure 22 shows the pH values of the surficial soil samples. From this, it can be conceived that the topmost part (6^{th} step) was highly acidic, the 5^{th} step was acidic to alkaline, 4^{th} step was alkaline.

Chemical weathering was detected to a varying degree in the different parts of the cut slope by analyzing the results of visual inspection, mineralogy, and pH of the soil samples of the slope. Based on this analysis, the weathered profile of mudstone along the cut slope can be divided into some distinct zones following Chigira M., 1990. The zoning of the mudstone based on chemical weathering is presented in Table 5 and Table 6. The soil profile along BH 1-1 was divided into three zones, W1, W2 and W3 (Table 5) based on the colour of the soil samples and weathered states obtained from soil boring. W1 represents the heavily weathered zone above 3.0 m. W2 is the zone of moderate weathering which is situated below 3.0 m. W3 marks the zone in the deeper part of the cut slope where the mudstone is weakly weathered and comparatively intact than the surficial area of the slope. Along this borehole, up to about 2.5 m below the surface, smectite content is very high, chlorite content is decreasing, and calcite and pyrite content already disappeared. Within this depth, the pH of the soil is highly acidic compared to the alkaline pH of intact mudstone. These factors indicate the occurrence and completion of oxidation in this zone. Hence, up to 2.5 m depth below the surface is marked as the oxidized zone where the mudstone is heavily weathered. Zone of dissolution and fresh rock which continues below 2.5 m, is marked by the presence of smectite, chlorite, calcite, and pyrite, along with neutral to alkaline pH. The oxidation front is the transitional area between these two fronts. The dissolved zone described in Chigira M., 1990 could not be separated in the studied cut slope due to the small elevation of the cut

slope. In the lower part of the cut slope, borehole 2-1 was zoned as W3 using the same criteria which were followed for BH 1-1. In BH 2-1, the zone of dissolution and fresh rock only could be identified due to the presence of moderate to low smectite content, no significant reduction in chlorite, calcite, and pyrite content, along with alkaline pH. Similarly, samples collected from the slope surface in both the upper and lower part show clear signs of oxidization in the mineralogical analysis. Therefore, it can be stated that the surface of the slope is significantly weathered. In borehole 2-1 and the weathered samples collected from the surface had alkaline pH values. The presence of calcite in these areas acted as a buffering agent, making the pH values comparatively higher despite the environment being highly acidic (Chigira and Oyama, 1999).

Chemical weathering progressed more severely in the upper region than in the lower part of the cut slope. In the upper part, the depth of oxidation was found to be around 2.5 m which is above the water table, and in this depth, the oxidation process was completed within 50 years. On the other hand, in the lower part of the surface of the slope, more oxidation is expected to occur, and the oxidation depth is expected to be around 3.0 m from the surface. Dissolution is expected to continue in both parts below 3.0 m as water causes the dissolution of minerals (Tarbuck et al., 2014). Although both physical and chemical weathering will progress further below the water table, its severity will be reduced greatly compared to the weathered zone in the upper part of the slope. Hence dissolution zone will start from the groundwater table and continue in the deeper part of the cut slope indicating that 50 years is not enough for the completion of the dissolution process.

The sedimentation time of the soil in the upper part and the lower part is different, and the mudstone in the upper part is comparatively fresher. Thermal expansion is easier in the upper part of the cut slope due to low overburden pressure than in the lower part, so water can easily penetrate the mudstone in the upper part (Carroll, 1970) and expedite chemical weathering. Removal of calcite makes the mudstone porous (Merrill, 1897) which works as an agent in further chemical weathering in the upper part. Additionally, in the upper part, the weathering can progress in mudstone from the top of the cut slope in the downward direction as well as from the surface in the perpendicular direction towards the deeper part. But in the lower part, the weathering can progress in mudstone from the surficial area only. Concrete linings and drainage systems to reduce pore water pressure and increase slope stability

are present at the top of each step. This hinders the progression of weathering from the top in each step. All these phenomena are the factors contributing to the greater extent of weathering in the upper part than the lower part of the cut slope.

5.3 Correlation between chemical and mechanical weathering

From the visual inspection, mineralogy, and mechanical evaluation of soil properties collected from the boreholes, the progression of chemical and physical weathering in the cut slope took place within 50 years after the excavation was discovered. From the analysis, it was observed that the weakening of the surface due to mechanical weathering is almost similar in both the upper and lower parts of the slope. The upper part of the slope is more chemically weathered than the lower part. The direction of the progression of weathering is perpendicular from the surface to the deeper part. It can be stated that the mudstone in the topmost part of the slope was chemically weathered before the excavation, and physical weathering started after the excavation. After the excavation, due to the stress release and exposure of the fresh rock to the environment, both chemical and physical weathering started from the cut surface and propagated in the perpendicular direction of the surface. One remarkable observation was the coincidence of the significant reduction of strength, stiffness, and density of the mudstone up to the depth of the chemically weathered zone. In the slope, up to the depth of 2.5 -3.0 m from the surface, chemical weathering is significant. Reduction in uniaxial compressive strength from the intact mudstone was observed only up to this depth. The reduction of stiffness was also greater in this depth compared to the intact mudstone. These observations confirm that chemical weathering affects the progression of physical weathering in the cut slope. In the depths where calcite was removed completely or decreased due to chemical weathering, the density of the mudstone was significantly reduced (Figure 15). From this, it can be stated that the depth of 2.5 – 3.0 m below the surface will be the zone of oxidation all over the cut slope area with time. Until this depth, further extensive chemical weathering is expected in the lower part of the slope until the condition becomes similar to the upper part. Further reduction in strength up to this depth is expected. Reduction of stiffness is also expected to be severe in this depth, although stiffness reduction will propagate in greater depth.

5.4 Effect of weathering on the stability of the slope

An oxidized zone in the cut slope can lead to a landslide (Chigira, 1990, Veder, 1981). (Bhattarai et al., 2007) have found the presence of smectite at sheared part of the mudstone slope. Simulation of long-term slope stability based on the test results obtained from this site is discussed in Chapter 6. It has shown that the weathered zone along the surface of the cut slope has the possibility of deformation despite having a higher safety factor for the entire slope.

5.5 Accelerated weathering test

Evidence of both mechanical and chemical weathering was found at Yoshida slope. To confirm the observations from the field, an artificial simulation of the chemically weathered mudstone from its intact state was attempted in the laboratory. The objective of this test was to check if the weathering of the mudstone can be introduced and accelerated by creating an artificial acidic environment for an intact specimen. The aim was to start the dissolution of pyrite, calcite, chlorite, and the development of smectite to confirm the occurrence of chemical weathering in nonweathered mudstone along with the pH change of the mudstone from alkaline to acidic. No mechanical tests to check the changes in the strength properties were conducted. Intact mudstone specimens from Zushi and Yoshida were taken from boreholes and observed throughout the process.

5.5.1 Methodology

Intact nonweathered mudstone from the deeper part of the slope of Yoshida and Zushi was selected for the test in the laboratory. Sample from 9.6 m depth at Yoshida (BH 3-1 B) (Figure 8) and from 12.0 m depth at Zushi (BH B1) (Figure 9) was taken. XRD tests of these samples were carried out to confirm that the samples did not contain any smectite but had pyrite, calcite, and chlorite. The total workflow of the test is shown in Figure 23. After selecting the mudstone specimens, they were powdered and sieved through a 53 μm sieve.

In the field, acid rain plays a big role in the dissolution of minerals and initiating chemical weathering (Hawkins, Lawrence, Privett, 1988). 0.05 mol/L (0.1 N) H_2SO_4 (Sulfuric acid) was used in this test to create the acidic environment artificially. To accelerate the weathering process, the acid of pH 2 was used. For this purpose, an Acid solution of 100 ml, 500 ml, 750 ml, 1000 ml, 1500 ml, 2000

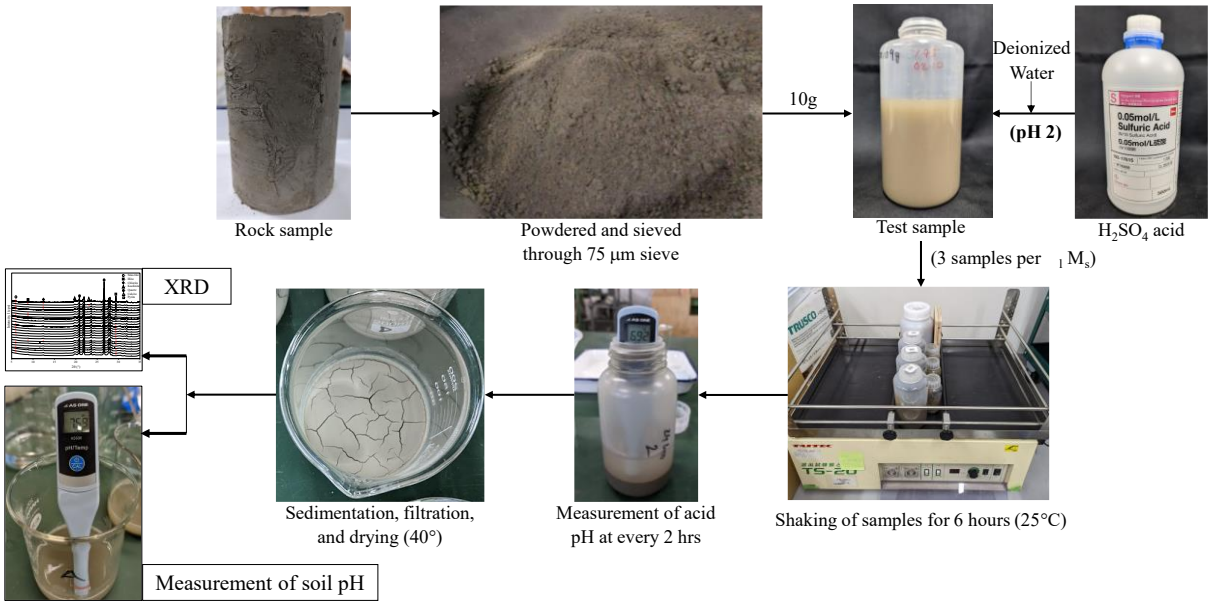

Figure 23 Workflow of the accelerated weathering test

ml, and 3000 ml volume (V_l) containing deionized water and 10% H_2SO_4 was prepared, each of them having a pH of 2. The volume of the sulfuric acid was increased gradually to achieve the end of the chemical reactions between acid and mudstone and to make sure that all the mudstone samples reacted with acid.

Test samples were prepared by taking 10g mass (M_s) of powdered sample and mixing it with different volumes (V_l) of acid in plastic containers. Observations were made for different liquid volume to soil mass ratios V_l/M_s. Three samples were made for each V_l/M_s ratio to ensure the repeatability of the test. Immediately after preparing the samples, they were placed on a shaking table. Samples were shaken for six hours at 25°C to ensure homogeneous mixing of the soil with the acid. On the way of the shaking, the pH of the liquid was measured every two hours, which is fundamentally the pH of the acid. After six hours, the samples were removed from the shaking table and left for the sedimentation of the soil at the bottom of the containers. Once sedimented, the liquid and the solid parts were separated through filtration using filter paper. The filtered soil was dried in the oven at 40°C until complete evaporation of liquid. The drying process took about three to four days. The dried soil was then divided into two parts. One part was used to check the mineralogy by XRD following the process described in section 4.2.1, and another part was used to check the pH of the mudstone following the process

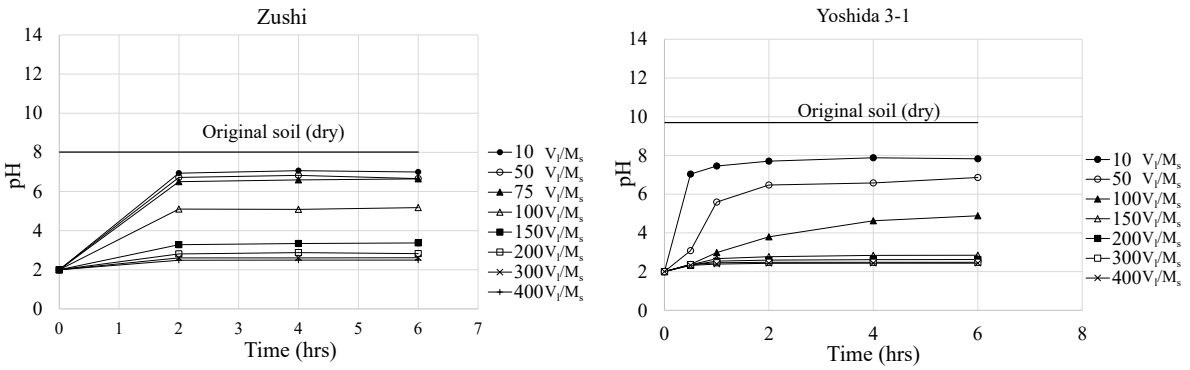

Figure 24 Determination of time required for shaking the samples

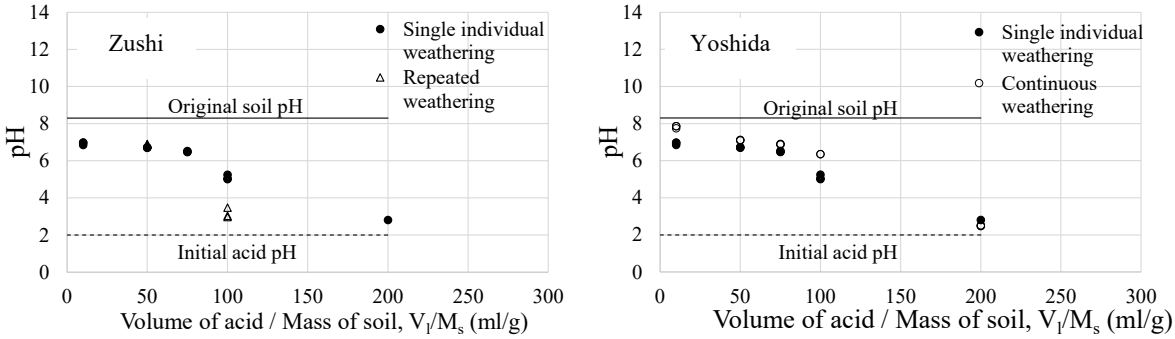

(a) (b)

Figure 25 Confirmation of the repeatability of the results

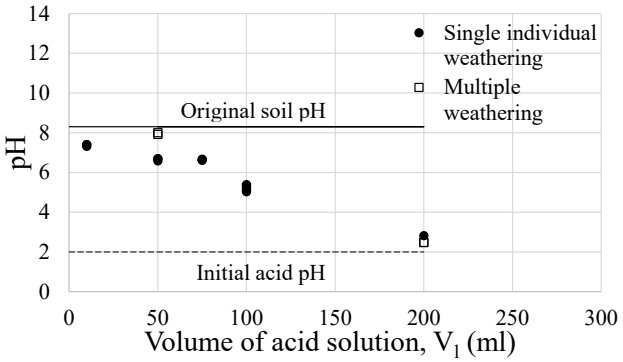

Figure 26 Confirmation of the amount of acid used in the samples

described in section 4.2.2.

5.5.2 Validation of the test procedure

Validation of the test method was verified by confirming the required wetting time duration for the test, repeatability of the outcome, and quantity of the acid required in the sample.

5.5.2.2 Time duration of the test

One of the important factors in conducting the test is to identify how long it is needed to shake samples to ensure complete mixing and chemical reaction of the powdered mudstone and the acid solution. Trial tests were conducted for this purpose. Initially, samples from Zushi were taken for 10, 50, 75, 100, 150, 200, 300, and 400 V_l/M_s (Figure 24). The samples were mixed using the shaking table for six hours continuously. On the way to the shaking, the shaking table was stopped every two hours to measure the pH of the samples. The results from Zushi in Figure 24 showed that starting from the initial pH of the samples (pH 2), all of the samples with different V_l/M_s ratios showed an increase in pH value which finally reached an asymptotic state of very low pH variation after two hours of shaking time. To confirm this statement, the same experiment was conducted with the specimen from the Yoshida slope (Figure 24). In this case, pH change was recorded at 15 minutes, 30 minutes and one hour after the start of the shaking along with the data of 2 – 6 hours. It was observed that the pH of the samples rapidly increased from their initial value until 2 hours of shaking. It becomes asymptotic afterwards. Hence it can be stated that shaking the samples continuously for two hours is enough to ensure the proper mixing of the powdered mudstone, and this duration is enough to complete most of the chemical reactions occurring in the samples.

5.5.2.2 Repeatability

The repeatability of the test results was confirmed by weathering the samples in different methods for the same V_l/M_s ratio and comparing them together. Generally, each sample for each V_l/M_s ratio is prepared individually by mixing the intact ground mudstone with the required amount of acid and deionized water. After that, a full cycle of test flow described in section 5.5.1 is conducted. This is denoted as “single individual weathering” in this test. Samples were prepared in two other methods as well to check the repeatability of the results. One is denoted as “repeated weathering”. In this case, three samples of 50 V_l/M_s were prepared with 500ml 10% H_2SO_4 and 10g of soil from Zushi, and tests were conducted until the sedimentation, filtration, and drying stage. With the dried soil, instead of checking the soil pH and XRD, an additional 500 ml of 10% H_2SO_4 was added to it. Hence, the final amount of acid applied to the soil is 1000 ml for a specific. The aim here was to check if similar results can be

obtained for a specific V_l/M_s ratio if its half ratio is repeated. In this case, the 50 V_l/M_s ratio is repeated once with the same soil to replicate the 100 V_l/M_s ratio. Figure 25 (a) shows the comparison of single weathering and repeated weathering. At 50 V_l/M_s, both single weathering and repeated weathering samples give the same pH. At 100 V_l/M_s, there is a difference in the absolute pH value of the acid. Repeated weathering samples gave lower pH than that of single individual weathering. But the decreasing tendency of the pH is the same. Another approach to check the repeatability of the results was "continuous weathering". In this case, instead of preparing the samples individually for each V_l/M_s ratio, three samples were prepared for 10 V_l/M_s with the intact mudstone from Zushi. Tests were run with these samples until the sedimentation, filtration, and drying stage (section 5.5.1). In the dried sample, additional deionized water of 10% H_2SO_4 was added to reach the next V_l/M_s ratio. Hence the test started at 10 V_l/M_s and continued to 50, 150, 100 and 200 V_l/M_s. Figure 25 (b) shows the comparison of single weathering and continuous weathering. The pH values of wetting liquid after six hours of shaking for both single weathering and continuous weathering are similar. The trend in the increase in the final pH value for both cases is also the same. Hence it was confirmed that, despite the process of weathering, for a specific V_l/M_s, the same amount of chemical weathering will occur to the mudstone and the repeatability of the test is confirmed.

The total amount of acid consumed by all the samples is the same, but the process of consumption is different. The main difference between repeated and continuous weathering is in repeated weathering, the sample was dried after the test, but in continuous weathering, the samples were not dried, and the test was continued by adding more acid. From this, the effect of drying on pH variation could be checked.

5.5.2.3 Quantity of acid

A trial test by varying the amount of acid for a specific V_l/M_s ratio was conducted. This set of tests is denoted as "multiple weathering". Powdered samples of intact mudstone from Zushi were taken for this. Three samples were prepared with 10g soil and 500ml 10% H_2SO_4 hence 50 V_l/M_s. These samples were shaken for six hours and sedimented, filtered, and dried (section 5.5.1). In the dried soil, 500 ml 10% H_2SO_4 and 500 ml deionized water were added. Hence, this sample became the same state

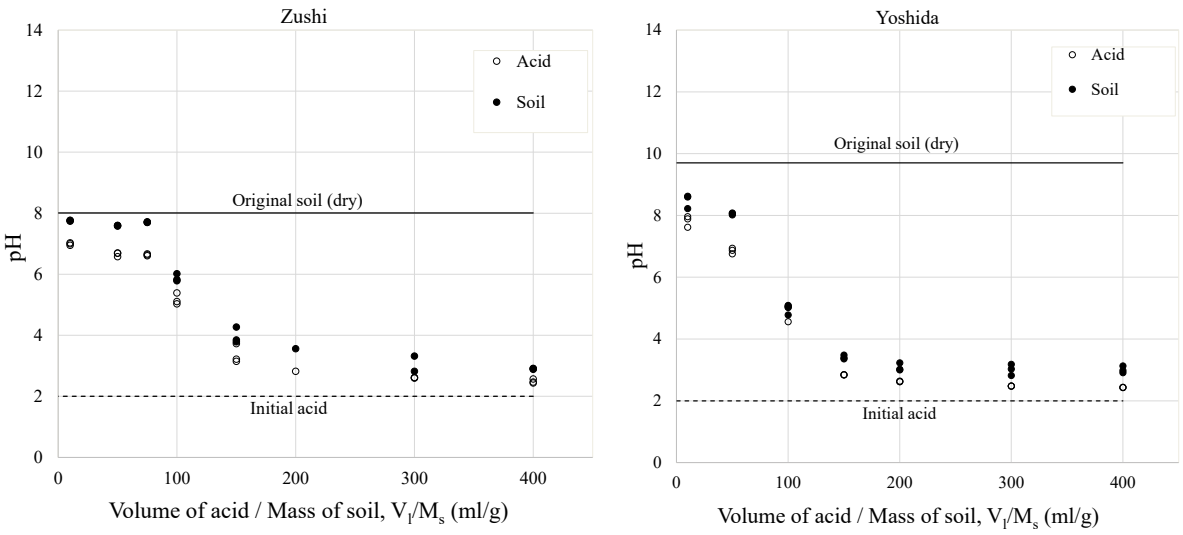

Figure 27 pH of samples vs Volume of acid / Mass of soil

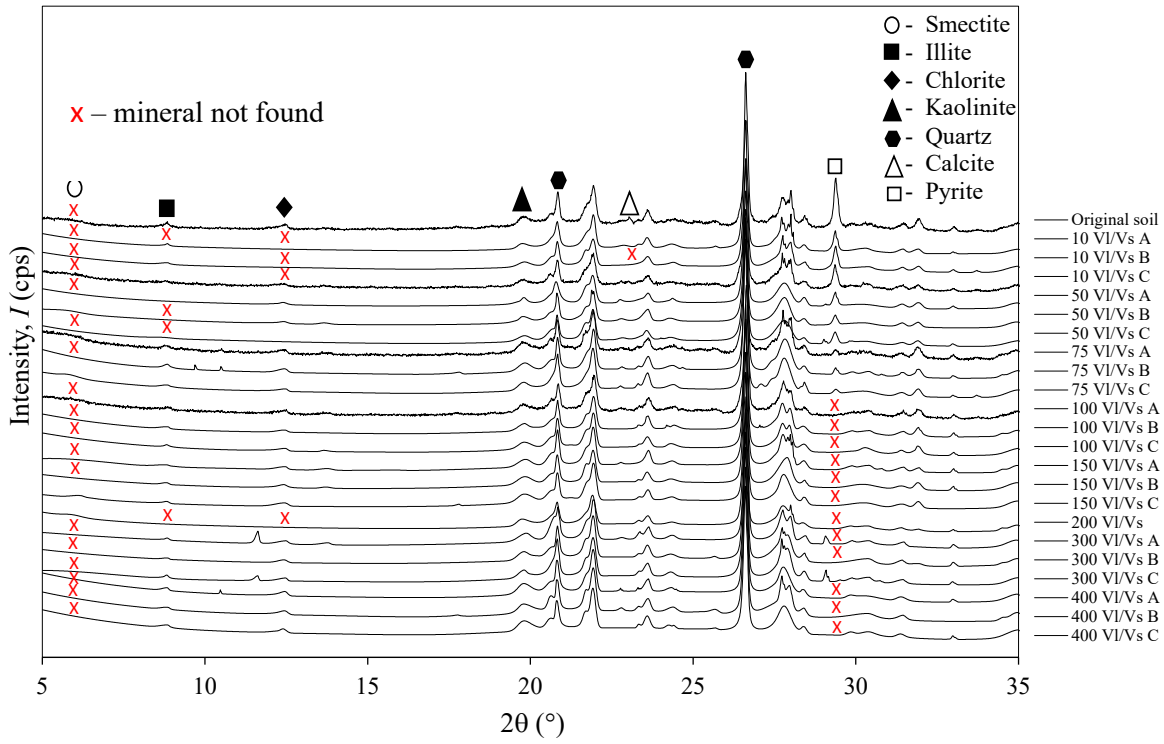

Figure 28 XRD intensity graph of the test samples from Zushi

as 100 V_l/M_s with an additional 500 ml of deionized water. The test cycle was run again until the sedimentation, filtration, and drying stages. With the dried sample, 1000 ml 10% H_2SO_4 and 1000 ml deionized water were added again. Hence, this sample became the same state as 200 V_l/M_s with an additional 1000 ml of deionized water. The test cycle was run again until the sedimentation, filtration, and drying stages. Figure 26 shows the comparison of the pH of the acid in single individual weathering and multiple weathering. At the point of 50 V_l/M_s ratio, the sample for both cases is the same in terms of preparation. Their pH varied slightly, though, mainly due to the sensitivity in sample preparation. In points 100 and 200 V_l/M_s, samples in the case of multiple weathering contained the same amount of extra deionized water to its acid volume compared to the single individual weathering case. But the pH value of the sample for both cases is similar. This indicated that in the test, the volume of acid is more important than the total volume of the wetting solution.

5.6 Observation of simulated chemical weathering

Several important observations were made from the trends of pH and mineralogical change through the accelerated weathering test in terms of the chemical weathering of mudstone. These observations are described in this section.

5.6.1 Variation of pH with acid volume

shows the variation of the pH of the intact mudstone from Zushi and Yoshida with the application of increasing amounts of acid volume. The pH of the original intact mudstone at Zushi slope is 8.01, and at Yoshida is 9.7. In both cases, samples were prepared from fresh mudstone and single individual weathering was applied. Figure 27 represents the pH of the acid at the end of the test (after six hours of shaking) and the pH of the soil obtained at the end of the test (section 5.5.1). For both Zushi and Yoshida, the pH of wetting liquid and soil increased largely at a low volume of acid. A gradual reduction at the increase of pH occurs at the increase in the volume of acid, which eventually becomes asymptotic. Soil pH at the end of the test was always found to be higher than the pH of its wetting liquid at each V_l/M_s ratio. An increase in the pH of the acid and a decrease in the pH of the mudstone confirms the occurrence of chemical weathering. At the application of a low volume of acid, acid is fully consumed by mudstone, and it remains alkaline. With an increase in the volume of acid, acid

consumption reduces, and the pH of mudstone reduces gradually to an asymptotic value. pH of acid at the end of the test tends to become acidic with the increase in V_l/M_s ratio, indicating that the amount of surplus acid is increasing in the samples. Hence it is clear that the larger the volume of acid, the more chemical weathering is accelerated in the mudstone. The final pH of acid in the samples at the asymptotic state is always higher than its initial pH of 2. This indicates that, in the field, the pH of the mudstone will always be higher than the strongest acid rain it will ever experience. Mudstone from Yoshida shows a faster reduction in pH compared to Zushi. This indicates that the mudstone in Yoshida slope is more susceptible to chemical weathering.

5.6.2 Variation of minerals

XRD test was conducted according to the method described in the section for the original intact mudstone and at the end of each cycle of testing for both Zushi and Yoshida. Figure 28 and Figure 29 present the X-ray intensity graphs obtained from the testing of Zushi and Yoshida samples, respectively. As three samples were prepared for each V_l/M_s ratio, they were marked as A, B, and C. Figure 28 and Figure 29 show that the intact nonweathered mudstone sample marked as "original soil" did not contain any smectite and contained an abundance of chlorite, calcite and pyrite along with illite, kaolinite and quartz. XRD analysis gives information regarding the presence and absence as well as quantitative changes of minerals. In both Zushi and Yoshida samples, no significant change was noticed in the quartz, illite, and kaolinite. As the amount of acid application increased, some samples showed the disappearance of chlorite and calcite, although a reduction of their quantity is not clearly conceivable. Clear reduction and disappearance of the quantity of pyrite at the application of 1000 ml acid are observed in both Zushi and Yoshida samples. The reduction in the peak for pyrite in Figure 28 and Figure 29 indicates the reduction in their quantity compared to the original specimen. Hence it can be stated that pyrite has been dissolving along the way with an increase in acid volume. Dissolution and disappearance of pyrite thus confirm the initiation and progress of chemical weathering in the test. Although smectite was expected to develop with the dissolution and disappearance of pyrite, its development is not clearly visible in Zushi samples. At the large application of acid in Yoshida samples, it showed minor development of smectite, although its quantity is difficult to calculate from the intensity.

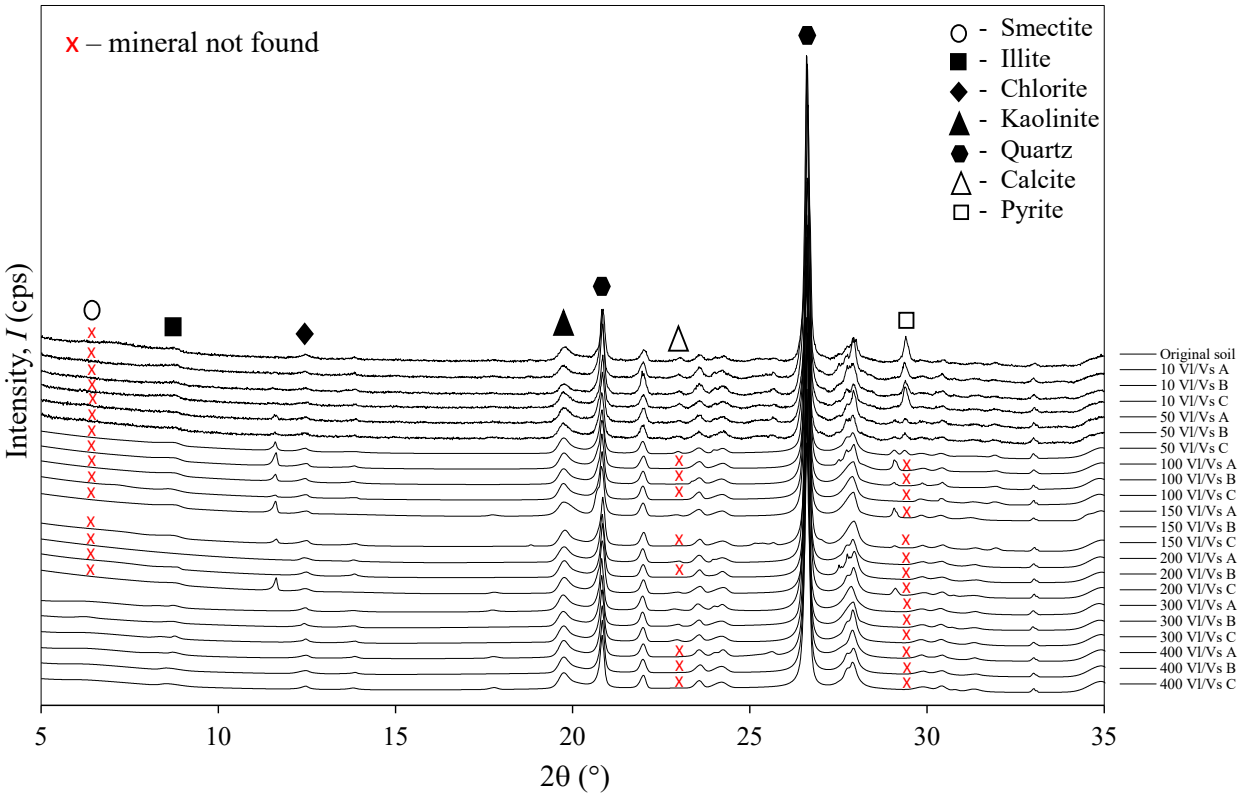

Figure 29 XRD intensity graph of the test samples from Yoshida

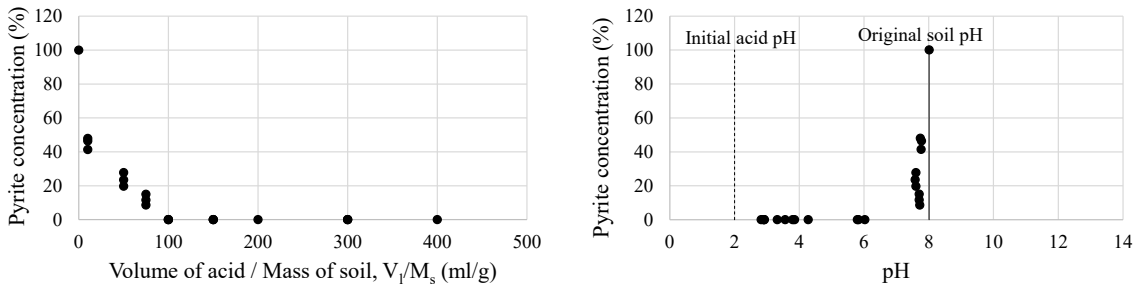

Figure 30 Variation of Pyrite concentration with V_l/M_s and pH in Zushi

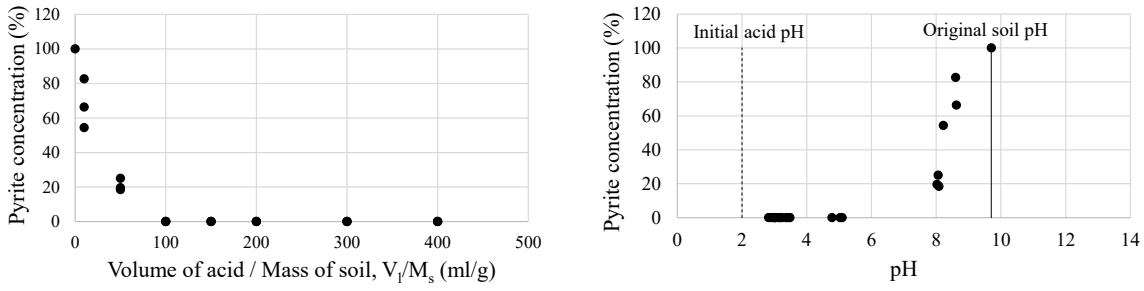

Figure 31 Variation of Pyrite concentration with V_l/M_s and pH in Yoshida

graph. As there is still abundant chlorite available in the sample, it is understandable that the process of smectite development from chlorite is not complete yet. From the observations above, it can be stated that this accelerated weathering method was successful in capturing the mineralogical changes that generally occur during mudstone weathering. Thus, this method can be applied in the practical field to understand the chemical weathering mechanism of mudstone from different locations by interpreting the mineralogical state.

5.6.3 Variation of pyrite with acid

Figure 30 and Figure 31 show the changes in the qualitative reduction in the pyrite content with the application of increasing amounts of acid in the mudstone of the slopes in Zushi and Yoshida. This qualitative amount was identified by calculating relative intensity, I_r from the intensity curves following the procedure explained in section 4.2.1. From these figures, it was observed that pyrite was melting with the increase in the volume of acid. A direct link between pH reduction and the disappearance of pyrite was observed from these figures. The pH of the intact nonweathered mudstone is alkaline. With the application of acid and the increase of its volume to the sample, the pH of the mudstone reduces gradually to a neutral pH. With this decrease in pH, the pyrite content of the sample reduces simultaneously. An important observation here is that when the pH of the soil becomes acidic from neutral, pyrite content disappears. In both Zushi and Yoshida samples, this phenomenon occurs with the application of 1000 ml of acid. pH reduction was drastic once the pyrite disappeared in the samples. It can be said that at the application of a low volume of acid, acid is consumed by the chemical reactions needed for pyrite dissolution. Primarily, pyrite oxidation initiates the dissolution of calcite and chlorite which causes further chemical weathering in the mudstone. With the increase in acid volume, pyrite is completely dissolved from the mudstone and the pH of the applied acid dominates in the sample. Hence it can be stated that the field conditions of chemical weathering could be reproduced in the laboratory by this accelerated weathering test. The test results also ensure that the pH of the mudstone is an important measure in detecting the weathering state. Chemical weathering can start without significant variation in pH though. As long as there is available pyrite to dissolve in the mudstone, the pH will remain alkaline. Hence, acidic pH indicates pyrite is completely removed from the mudstone and its

chemical weathering is approaching an end.

Consistency between the results of the Yoshida and Zushi, which are situated in different locations and have difference in the formation, indicates that this newly developed accelerated weathering test has high repeatability. Hence, this test can be successfully applied in the case of other mudstone from various locations and having different composition. The pH and mineralogical condition obtained from the accelerated test and that observed in the field are consistent. The results obtained from this test implies that, in the field, we can perform a quick check of present chemical weathering by checking the pH and mineralogy of the mudstone from the surface and estimate the state of weathering condition. One fundamental difference of this test from the other research mentioned in the literature review is, this test shows the direct relationship between the pH, mineralogy, and the acid volume as we get the reduction of pyrite and changes in pH with the increase in acid volume. This data can be further interpreted in the future as the consumption of acid volume by pyrite in the mudstone with annual rainfall and can be related to the quantitative amount of chemical weathering each year.

6. NUMERICAL SIMULATION OF WEATHERED CUT SLOPE STABILITY

6.1 Outline of the simulation

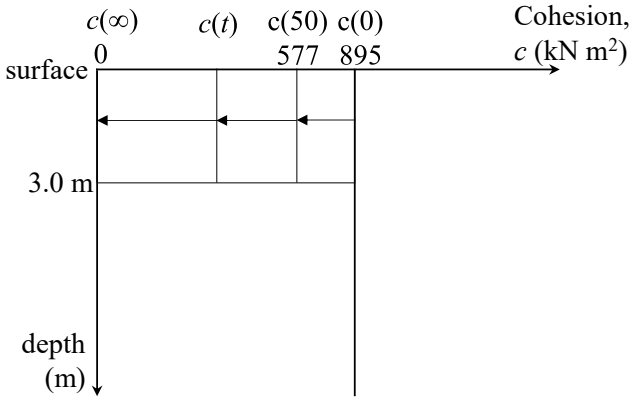

Figure 32 Schematic diagram of reduction of the strength of mudstone with time due to weathering.

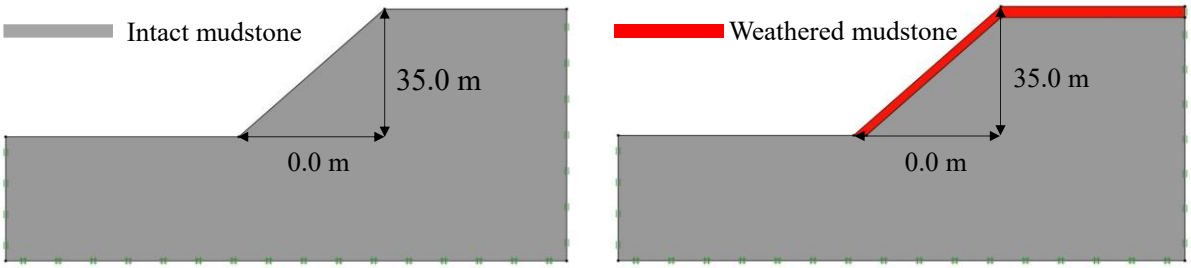

Figure 33 Simulation conditions

The relationship between the strength parameters of intact rock and changed parameters of the intact rock induced by weathering within 50 years was obtained. From this relationship, the future possible behaviour of the cut slope was extrapolated. Finally, the variation in the factor of safety and change in the failure mechanism of the slope with time was simulated by limit analysis using the rigid-plastic finite element method. A finite element program, "OPTUM G2", was used for running the strength and deformation simulation in a simplified geometry of the slope Figure 33.

6.1.1 Failure criteria of weak rock

Mohr-Coulomb's failure criteria for the soil were combined with a failure criterion based on weathering of the mudstone with time to evaluate the state of the stability of the cut slope due to weathering with time.

6.1.1.1 Failure criteria based on weathering

Gradual reduction of the strength of the mudstone with time induced by weathering was modelled considering the following assumptions based on the field and laboratory test results:

- Immediately after the excavation, the strength of the mudstone was uniform all over the slope and was the same as the intact part of the slope.
- Over the years, up to the weathered depth of 3.0 m below the surface (oxidized zone), the strength of the mudstone will decrease. In the field, full disintegration of the weathered mudstone was observed at the surface of the slope. Hence eventually, in this depth, the strength will become zero. Below 3.0 m, the strength of the rock will be stable and remain similar to its initial strength.
- In the final stage of weathering in this depth, mudstone will be fully disintegrated into the sedimentary deposit and have no cohesion. However, the frictional value will be the same as the intact rock (30°). A similar assumption was made by Utili and Crosta, 2011 for the analysis of weathering in natural slopes. Bhattarai et al., 2007 also showed that in the case of the depth-wise weathering analysis of the mudstone slope at Mukohidehara, Niigata, the angle of friction above the ground water fluctuation zone did not vary much despite significant physical weathering. Ping et al., 2023 also showed that, despite the dissolution of minerals in the mudstone due to weathering, the reduction in cohesion is much more significant than the change in the angle of friction. Eberhardt et al. 2005 and Hou et al. 2014 also came to a similar conclusion of changes in cohesion being the dominant factor due to weathering compared to the angle of friction.
- Due to the presence of the highway at the bottom of the slope, no change in strength due to weathering in the mudstone was considered below the highway pavement.

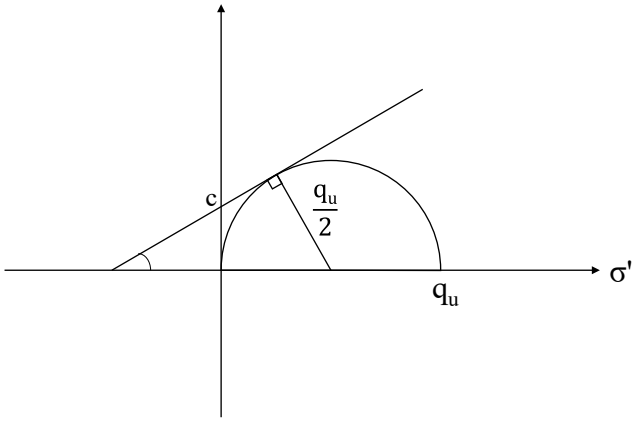

Figure 34 Mohr's failure envelope

Considering these assumptions, the gradual change in the strength of the slope with time due to weathering is represented in Figure 32. Cohesion, c, was assumed to be constant at c(0) in the intact zone over 3.0 m depth. Meanwhile, it was described by a monotonic-decreasing function c(t) in the weathered zone up to the depth of 3.0 m to consider the weathering-induced reduction of the strength with time, t (years). Initial cohesion immediately after the excavation, c(0), and the current cohesion value at 50 years after the excavation, c(50), were obtained from laboratory test data of the intact and weathered samples, respectively. For the weathering zone, it was assumed that the cohesion of the mudstone reduces with time and finally approaches zero. By deducing the asymptotic reduction in cohesion in the weathering zone, the cohesion at the time *t*, is given as follows.

$$c(t) = c_0 \exp(-kt) \tag{3}$$

Here, *c* is the cohesion of the mudstone corresponding to the time *t*, and c_0 is the cohesion of the intact mudstone.

Using the experimental data of intact samples and weathered samples at 50 years, the parameter *k* was determined.

6.1.1.2 Mohr-Coulomb failure criteria

Mohr-Coulomb failure criteria are simple and widely used failure criteria in slope stability analysis (Li et. al, 2009, Muntohar and Liao, 2009, Ivan and Ikuo, 2011). In this research, limit analysis of the concern slope was conducted using Mohr-Coulomb failure criteria. Using the OPTUM G2 software, strength reduction analysis was carried out to obtain the factor of safety of the slope for

different periods after the excavation of the slope. Equal reduction of the parameters c (cohesion) and tan φ (angle of friction) in Mohr-Coulomb criteria was performed in strength reduction analysis to induce a state of collapse. A strength-based factor of safety was obtained from the resulting factor using the formula:

$$FS = \frac{c}{c_{red}} = \frac{\tan\varphi}{\tan\varphi_{red}} \quad (4)$$

In this simulation, c values were obtained from the conversion of interpolated and extrapolated q_u (unconfined compressive strength) values using the following equation obtained from Mohr's failure envelope (Figure 34):

$$c\ (kN/m^2) = \frac{q_u}{2\cos\varphi}\ (1 - \sin\varphi) \quad (5)$$

φ value was assumed to be a constant of 30° for all the simulations. c and φ are reduced until failure occurs to obtain FS at each time step of the analysis. Here,

c, tan φ = at a certain time step, cohesion and angle of friction assumed from the weathering analysis

c_{red}, $\tan\varphi_{red}$ = at the same time step, gradually reduced cohesion and angle of friction to achieve failure and calculate FS.

6.1.2 Model for the Strength of rock

The rigid-plastic finite element modelling was used to perform a stability analysis of the slope from which the behaviour of the structure can be pictured. In this method, an assumption about the mode of the failure is not required. Simple strength parameters are enough to execute the stability analysis and failure mode with stress and strain rate distribution can be obtained easily. The following equations were satisfied for his analysis and strength reduction analysis for different periods and strength were conducted:

6.1.2.1 Governing equation

In the rigid-plastic analysis, materials show no deformation below the point of yield but at the yield point, it shows unlimited plastic deformation. Hence, the governing equation is formulated in

terms of the rate of displacement (velocities) and strain rates as total displacement and strains cannot be measured. The static equilibrium equation and boundary conditions are as follows:

$$\boldsymbol{\nabla}^{\mathrm{T}}\boldsymbol{\sigma} + \mathbf{b} = 0 \quad \text{in V} \tag{6}$$

$$\mathbf{P}^{\mathrm{T}}\boldsymbol{\sigma} = \mathbf{t} \quad \text{on } \mathrm{S}_{\sigma} \tag{7}$$

The constitutive relationship considering the associated flow rule is:

$$\mathrm{F}(\boldsymbol{\sigma}) \leq 0 \quad \text{(yield condition)} \tag{8}$$

$$\dot{\varepsilon}^{p} = \dot{\lambda}\frac{\partial F}{\partial \boldsymbol{\sigma}} \quad \text{where } \dot{\lambda} \geq 0 \tag{9}$$

Here, $\dot{\varepsilon}^{p}$ is denoted for plastic strain rates and $\dot{\lambda}$ is a plastic multiplier. The complimentary condition that needs to be satisfied always is:

$$\dot{\lambda}\mathrm{F}(\boldsymbol{\sigma}) = 0 \tag{10}$$

The compatibility equation for the modelling is:

$$\dot{\boldsymbol{\varepsilon}}^{\mathbf{p}} = \boldsymbol{\nabla}\dot{\mathbf{u}} \tag{11}$$

Here,

σ: stress; **b**: body force; **t**: traction force; F: yield criteria; u̇: displacement rate;

$\dot{\varepsilon}^{p}$: plastic strain rate; $\dot{\lambda}$: plastic multiplier; V: Solid volume; S: Solid boundary;

S_{σ} : Neumann boundary (where tractions are prescribed)

6.1.2.2 Limit analysis using the lower and upper bound principle

Limit analysis was performed to evaluate the collapse load of the cut slope. The lower bound principle gives a lower bound of the exact collapse load and the upper bound principle gives an upper bound. Hence, the exact collapse load can be bracketed using these two principles and a more realistic analysis can be done. In this software, strength reduction analysis of the slope was performed using these two principles separately to get the upper and lower bound of the factor of safety. The mean value of the factor of safety was taken as a solution afterwards.

Governing equations in terms of lower bound principle:

Maximizing collapse multiplier, α (the factor by which the multiplier loads need to be amplified to cause collapse) subjected to:

$$\nabla^{T}\boldsymbol{\sigma} + \alpha\mathbf{b} = 0 \quad \text{in V} \tag{17}$$

$$\mathbf{P}^{T}\boldsymbol{\sigma} = \mathbf{t} \quad \text{on } S_{\sigma} \tag{18}$$

$$\mathbf{F}^{T}\boldsymbol{\sigma} - \mathbf{k} + \mathbf{s} = \mathbf{0}, \quad \mathbf{s} \geq 0 \tag{19}$$

Governing equations in terms of upper bound principle:

Minimizing

$$\int_{V}\mathbf{k}^{T}\dot{\boldsymbol{\lambda}}\,dV - \int_{V}\alpha\mathbf{b}^{T}\dot{\mathbf{u}}\,dV \tag{20}$$

Subjected to:

$$\nabla\dot{\mathbf{u}} = \mathbf{F}\,\dot{\boldsymbol{\lambda}}, \quad \dot{\boldsymbol{\lambda}} \geq 0, \int_{S_{\sigma}}\mathbf{t}^{T}\dot{\mathbf{u}}\,dS = 1 \tag{21}$$

6.1.2.3 Input parameters

The rise and run of the slope were taken as 35.0 m and 40.0 m with a slope angle of 41.2° (Figure 33). The slope was fully supported at the bottom. Hence displacement in all directions at the bottom of the slope was constrained. On the sides of the slope, normal/roller support was provided. Hence, on the sides, any displacement in the normal direction was constrained; displacement only in the upward or downward direction was permitted. The obtained c values from Eq. 3 were used as input in the software. φ′value was kept constant at 30° for all the simulations and cohesion values were changed for the corresponding time in the weathering zone of 3.0 m. In the simulation, 1000 nos. of mesh were assumed to be uniformly distributed all over the geometry (Figure 35). Later, a convergence analysis was carried out where the mesh was gradually refined until achieving a stable solution.

6.2 The outcome of the simulation

To get the factor of safety of the concerned mudstone cut slope for different periods along with failure mode, a simulation was carried out following the process described in section 6.1. Using Eq. 3, changes in the current strength, c (kN/m^2) with time in the weathered depth of 3.0 m of the slope were obtained. The relationship is plotted and shown in Figure 36. Using the converted c and φ values, multiple strength reduction analysis was operated using the software. The results obtained are as follows:

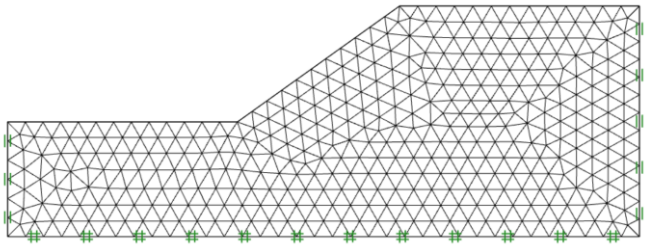

Figure 35 Initial mesh (1000 nos.)

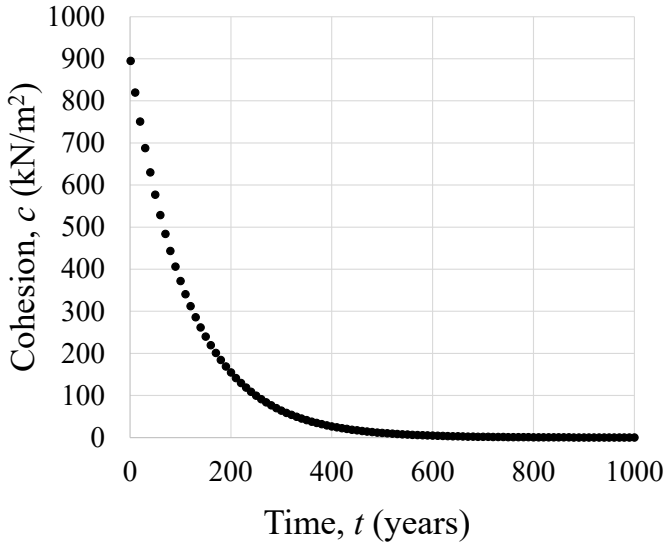

Figure 36 Variation of strength in surficial 3.0 m depth of mudstone with time

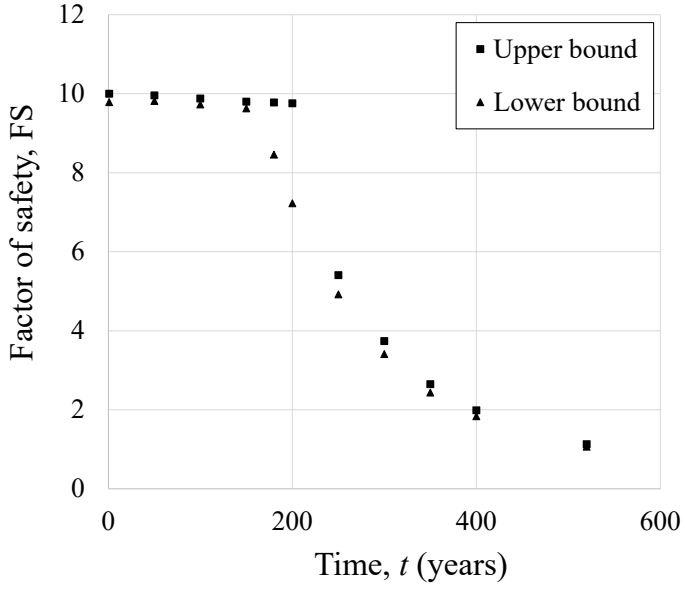

Figure 37 Variation of the factor of safety of the slope with time due to weathering

6.2.1 Variation in the factor of safety

Multiple slope stability analysis was conducted to obtain the gradual change of the factor of safety of the slope starting from its intact condition (right after excavation) until the weathered depth of 3.0 m from the surface has no cohesion (0 kN/m^2). In this analysis, as discussed in Chapter 6.1.2, the upper and lower limit of the factor of safety was obtained. The gradual decrease in safety factor due to weathering with time is shown in Figure 37. From this figure, it can be conceived that, until about 150 years, the slope will be stable and will have no significant effect on safety factor due to weathering. However, after 150 years, due to weathering, the factor of safety decreases rapidly, eventually becoming 1 after 500 years.

6.2.2 Variation in the mode of failure

The variation in the failure mode of the slope induced by time-dependent weathering can be clearly seen in Figure 38. This figure shows the critical plastic multiplier (λ) for upper and lower bound method for different periods of time after the excavation. The convergence of mesh around the failure zone at the end of the analysis is also visible in this figure. Initially, the FS of the slope is high, and the failure mode of the slope is the general rotational failure with a circular slip plane. However, with time, the failure mode changes. This simulation indicates (Figure 37) at around 180 years [c(180) = 184 kN/m^2], there is a significant decrease in the lower bound of FS and it indicates changes in failure mode. This condition reveals that, at this time period, the weathered zone is the most vulnerable and has a strong possibility of a landslide. Moreover, from this simulation (Figure 37), it is obtained that the FS of the slope becomes 1 after 500 years. From Figure 38, it was conceived that the shear failure would occur in the general circular slip plane. Moreover, there is a possibility of plastic deformation in the lower part of the surface of the slope. This clarifies the reason for the occurrence of deformation around BH 2-1 in 2016. Variation in stress vectors (σ_1,σ_3), strain rate vectors ($\dot{\varepsilon}_1$,$\dot{\varepsilon}_3$), and displacement vectors in both upper and lower bound limit analysis are shown in Figure 39, Figure 40, and Figure 41, respectively.

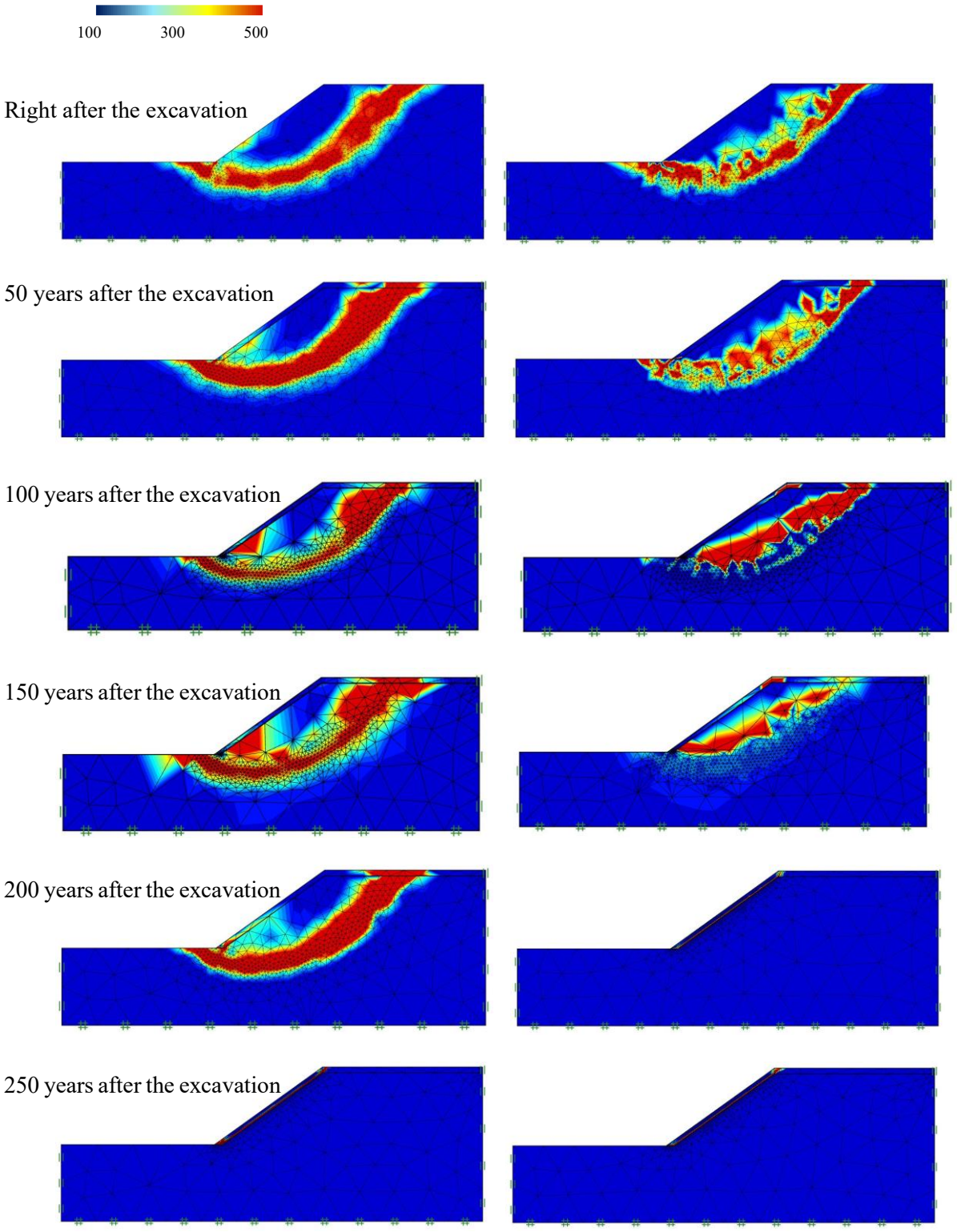

(a) Upper bound (b) Lower bound

Figure 38 Variation in plastic multiplier (λ) of the slope due to weathering with the different time

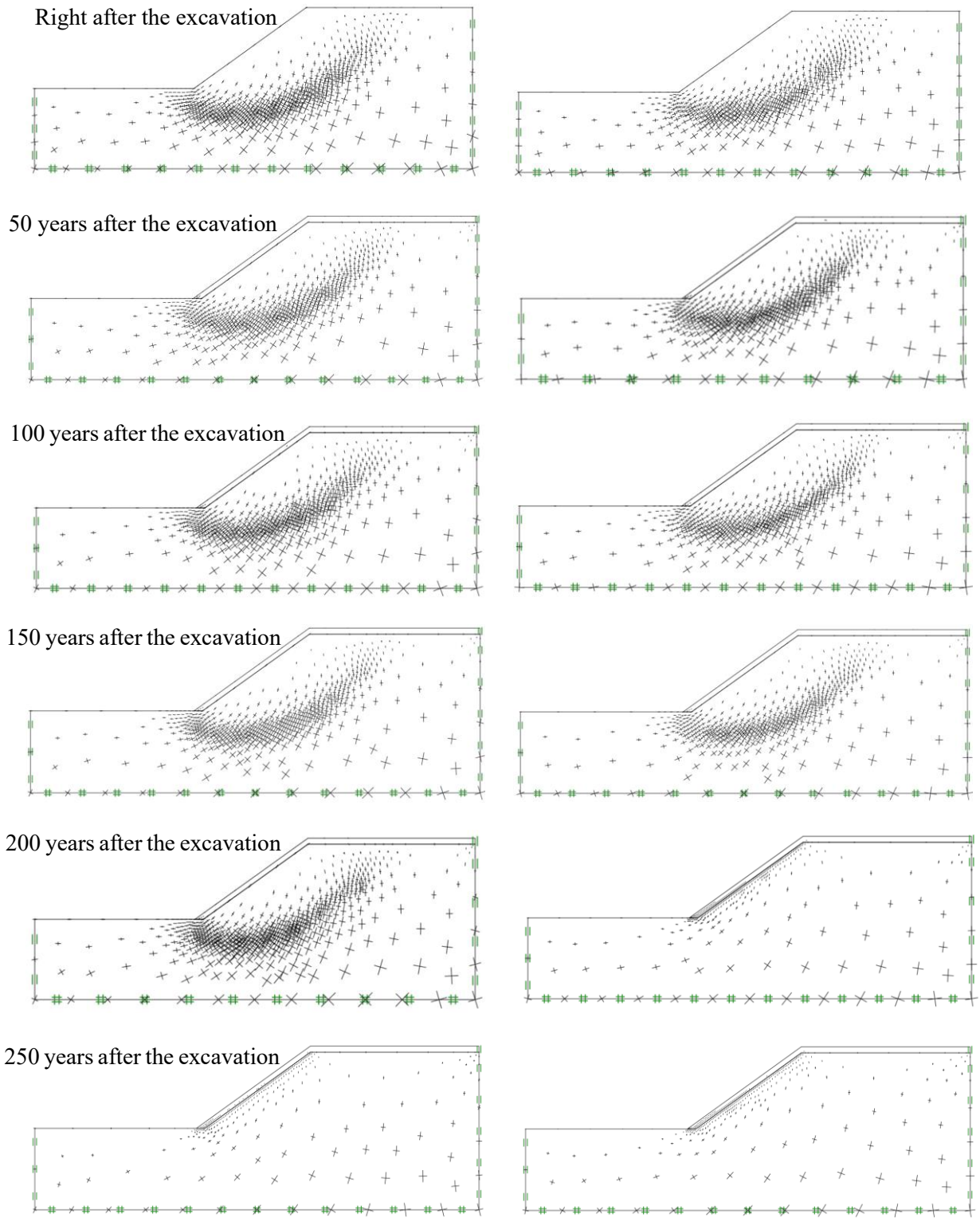

(a) Upper bound (b) Lower bound

Figure 39 Variation in stress vectors (σ_1, σ_3) of the slope due to weathering with different time span

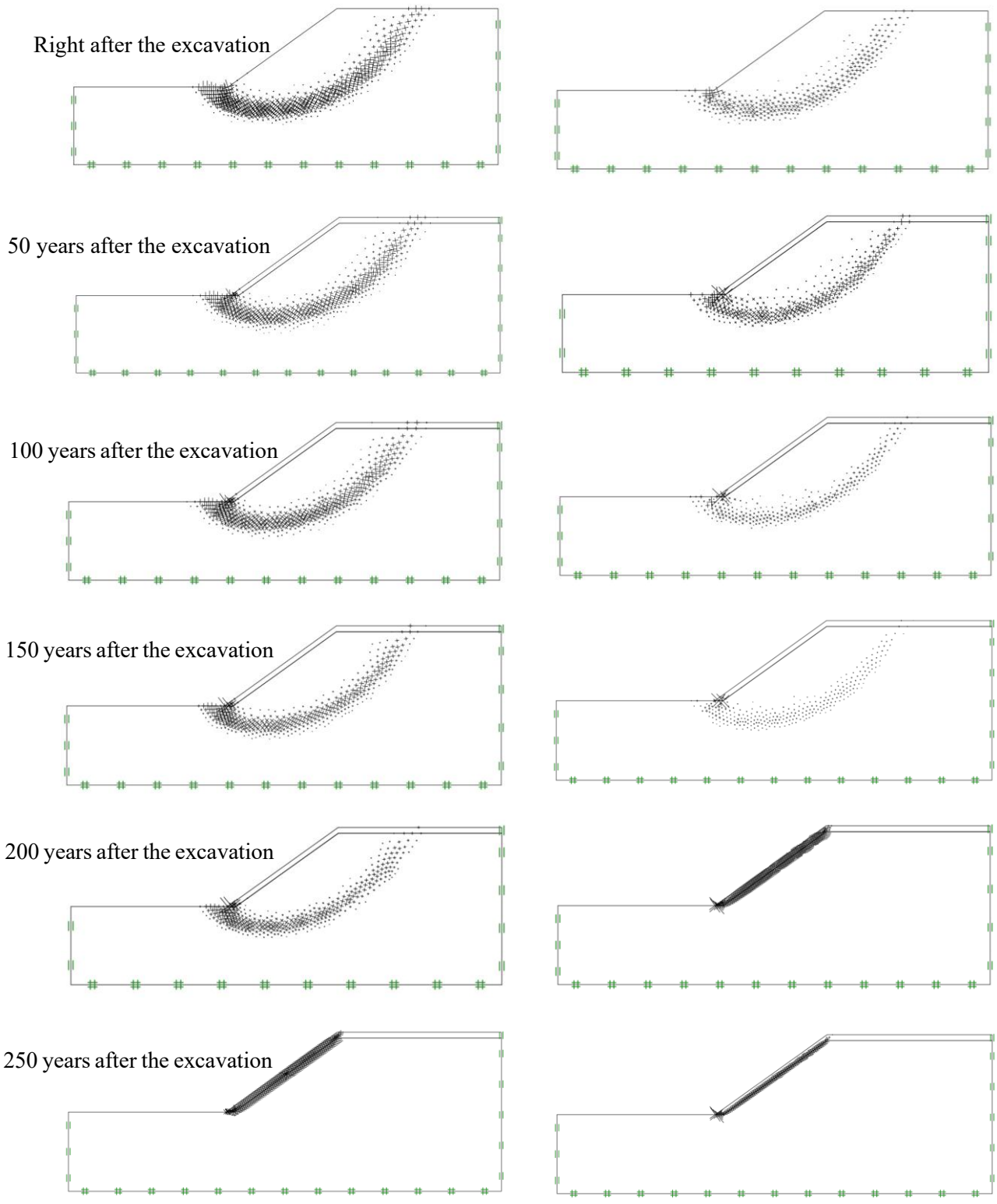

(a) Upper bound (b) Lower bound

Figure 40 Variation in strain rate vectors ($\dot{\varepsilon}_1$,$\dot{\varepsilon}_3$) of the slope due to weathering with the different time

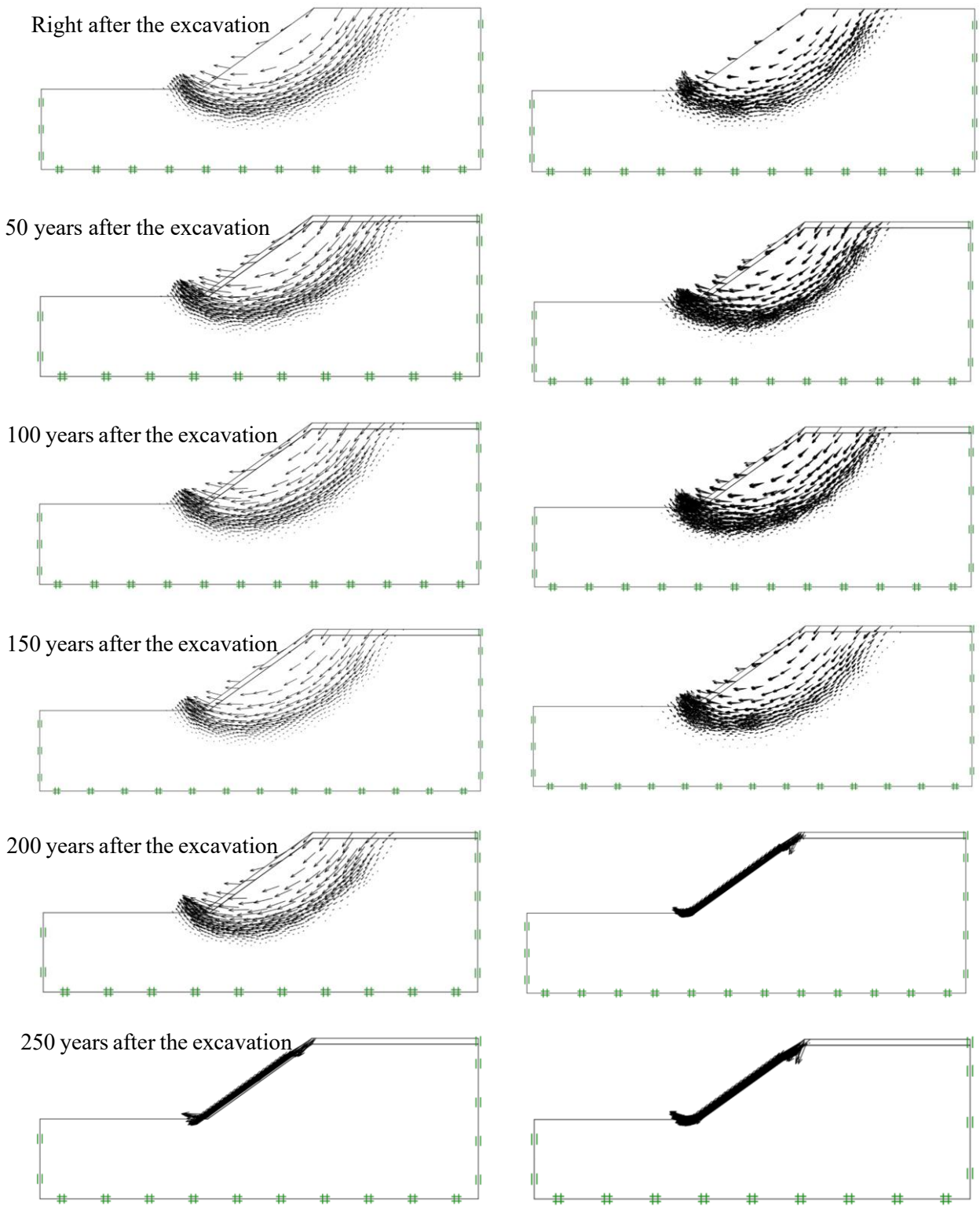

(a) Upper bound (b) Lower bound

Figure 41 Variation in displacement vectors of the slope due to weathering with the different time

Table 8 Dimensions of the slope considered for parametric study

	Height (m)	*Length (m)*	*Slope angle (°)*	*The ratio of the slope*
Case 1 (actual slope)	40.43	56.5	35.6	1 : 1.4
Case 2	40.43	86.7	25.0	1 : 2.1
Case 3	40.43	40.4	45.0	1 : 1.0
Case 4	40.43	28.3	55.0	1 : 0.7
Case 5	40.43	18.9	65.0	1 : 0.5
Case 6	30.43	42.5	35.6	1 : 1.4
Case 7	50.43	70.4	35.6	1 : 1.4
Case 8	60.43	84.4	35.6	1 : 1.4

6.3 Parametric study

A parametric study was conducted to check the effect of slope dimension in the slope stability and failure mode under the same consideration of strength reduction due to weathering with time.

Table 8 shows the eight different slope ratios considered for the simulation. Conditions of strength reduction with time and depth applied in the parametric study were the same as the actual slope. Only the slope angle and the height of the slope were varied for each case. The results of the parametric study were compared with the ones of the actual slope for upper and lower bound limit analysis in Figure 42 and Figure 43. Figure 42 and Figure 43 show the variation of FS in the cases where the slope angle and height of the slope are varied, respectively. Both figures show that the value of FS changes with the slope dimension. However, they show a similar trend in the failure mode and imply that, despite the dimensions of the slope, due to the progression of weathering with time after excavation, the failure mode of the slope changes, and the weathered zone becomes the most vulnerable zone.

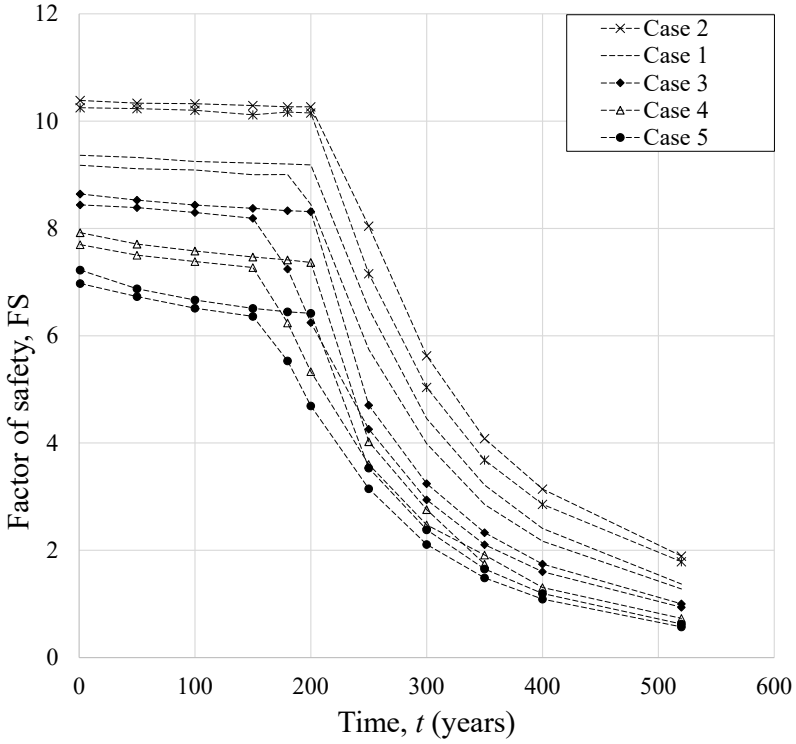

Figure 42 Parametric study of changes in slope angle (Cases 1-5)

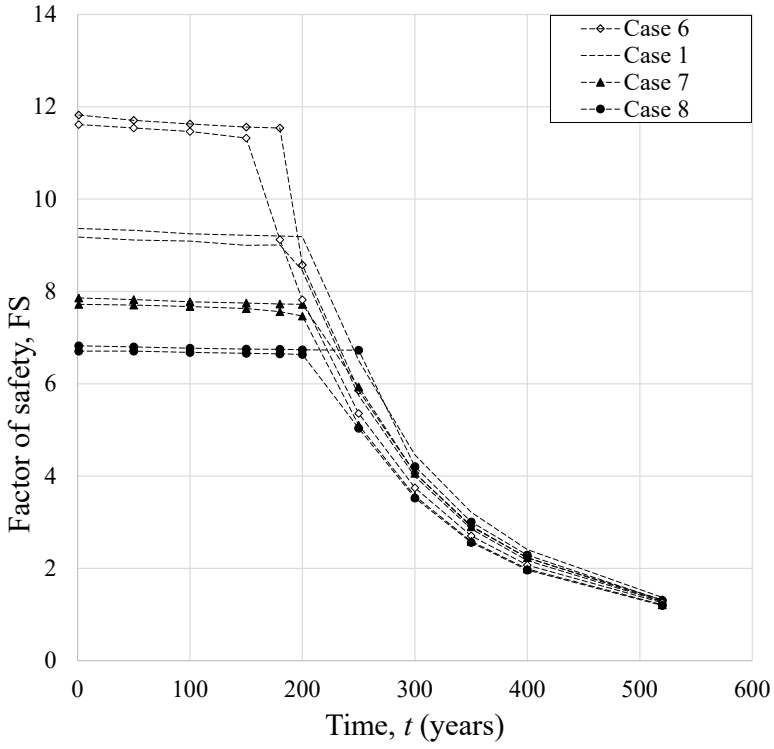

Figure 43 Parametric study of changes in slope height (Cases 1, 6-8)

7. COMBINED ANALYTICAL METHOD FOR WEATHERED CUT SLOPE STABILITY

In the RPFEM analysis, we did not have to assume the failure mode or slip line of the slope at a critical state before the analysis. The analysis gave us two possible modes of failure. One is the circular failure mode or rotational slip failure. Another one is transitional slip failure. The rotational slip failure mode is predominant when none to moderate surficial weathering is present at the slope. With time, surficial weathering becomes stronger, making the weathered zone lose its strength. Hence the weathered zone from the surface becomes dominant in slope instability causing transitional slip in the slope. We tried to create a simplified method using classical theories of slope stability analysis, which can be used as an alternative method to RPFEM simulation but can produce the same results. Bishop's method of slices was used for the rotational slip failure mode and the Infinite slope method was used for the transitional slip failure mode. These two hand calculation methods were combined to replicate the simulation results obtained from RPFEM.

7.1 Short-term stability - Bishop's method of slices

Bishop's method of slices (Bishop, 1955) is a very popular and useful method for slope stability analysis which analyses the critical failure state of a slope by dividing the slope into several slices. According to this method, the factor of safety, F of a slope can be obtained by calculating the ratio of the available shear strength of the soil in the slope to the strength of the slope required to maintain the plastic equilibrium. Hence, the mobilized shear strength, s is:

$$s = \frac{1}{F} \{ c' + (\sigma_n - u) \tan\varphi' \} \quad (22)$$

Where,

c' is cohesion and φ' is the angle of shearing resistance in terms of effective stress,

σ_n is total normal stress, u denotes pore pressure.

Some important assumptions considered in this method are:

- In plain strain condition, failure occurs in a circular arc (ABCD in Figure 44)
- The shear forces acting at the lateral sides of each slice are equal.

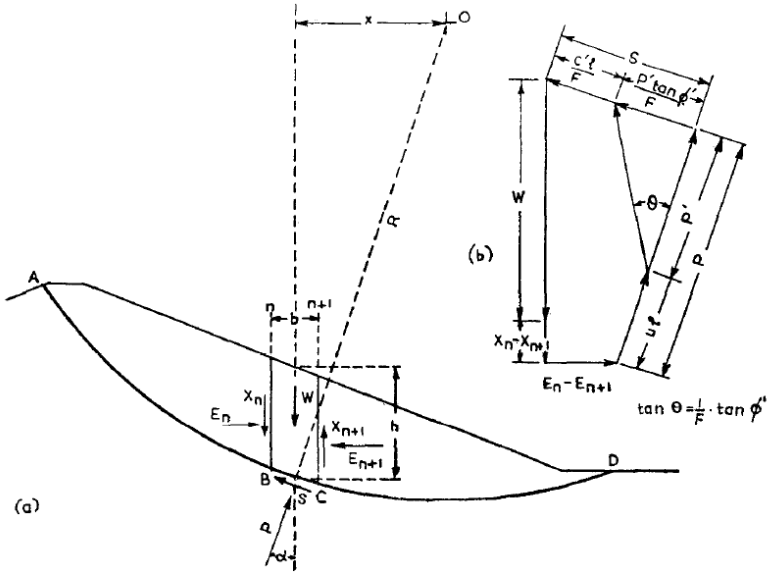

Figure 44 Forces in Bishop's method of slices [Bishop, 1955]

- If no external forces are acting on the surface of the slope, equilibrium must exist between the weight of the soil bounded by the circular arc ABCD of radius R and centre at O; and the resultant of the total forces acting on ABCD.

In Figure 44,

E_n, E_{n+1} : the resultants of the total horizontal forces on the sections n and n + 1 respectively

X_n, X_{n+1} : the vertical shear forces

W : the total weight of the slice of soil

P : the total normal force acting on its base

S : the shear force acting on its base

h : the height of the element

b : the breadth of the element

l : the length of BC

α : the angle between BC and the horizontal

x : the horizontal distance of the slice from the centre of rotation, O

Ensuring moment and horizontal force equilibrium for the total surface of failure with respect to O and vertical force equilibrium for each slice, F is determined from the iteration of a trial value. Using numerical analysis, the position of O is varied, and the critical failure surface is identified.

7.2 Long-term stability - Infinite Slope method

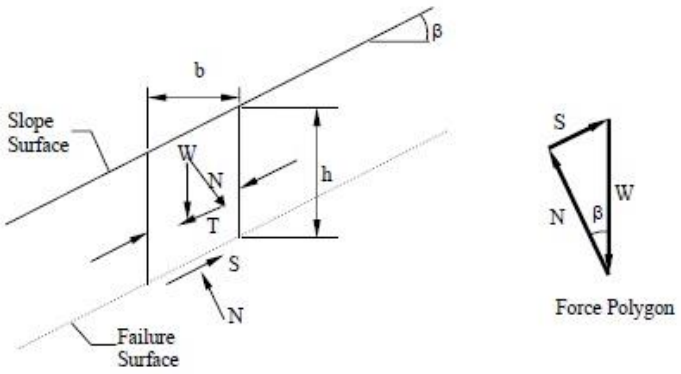

Figure 45 Forces in infinite slope method

Infinite slope stability analysis is a simplified method which considers the slope to be infinite and failure occurs along a plane parallel to the natural ground surface affected by gravitational forces acting on the soil mass (Figure 45). According to Brunsden and Prior, 1984, to calculate the factor of safety using infinite slope stability analysis, soil cohesion (c), the unit weight of soil (γ), the height of the slope (h), slope angle (β), and the angle of internal friction (φ) are needed. The factor of safety is calculated using the following equation:

$$F = \frac{c + (\gamma_{sat} - \gamma_w) \text{ x } tan(\varphi) \text{ x } cos^2(\beta) \text{ x } h}{\gamma_{sat} \text{ x } sin(\beta) \text{ x } cos(\beta) \text{ x } h} \quad (23)$$

7.3 Analytical model

FS of the slope was obtained for the slope from Bishop's method of slices and infinite slope method respectively using the same slope properties used in RPFEM analysis. Figure 46 shows the comparison of the obtained FS between the classical slope stability analysis methods (Bishop's method of slices and infinite slope) and RPFEM analysis. Bishop's method considers the failure of the entire slope without much concern for surficial failure. On the other hand, based on the assumptions of the infinite slope model, surficial failure of the slope due to a weakened weathered zone can be simulated. If we combine the results obtained from these two theories, we can see from the value of the FS (Figure 46), after the excavation of the slope, rotational or general failure of the slope is dominant. After about 150 years, surficial or transitional slip failure becomes dominant in the slope due to the weak weathered

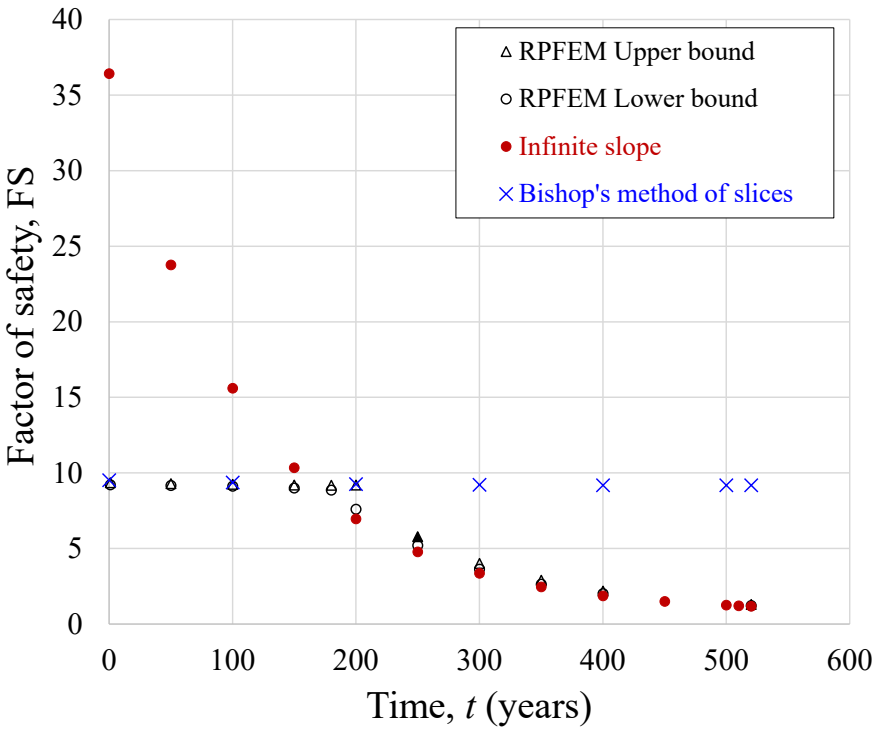

Figure 46 Comparison between RPFEM and simplified method

zone. The combination of the simplified method also indicated the change in the failure mode which we obtained from RPFEM earlier at a similar time after excavation. Moreover, the FS obtained from Bishop's method before the failure mode change and the FS from the infinite slope model after the failure mode change has good compliance with the FS obtained from RPFEM. Hence it can be said that this analytical method can be successfully applied as an alternative and simplified method to RPFEM to evaluate slope stability with weathering phenomenon.

8. CONCLUSIONS

From the evaluation of the properties of the mudstone cut slope at Tomei expressway in Yoshida district, the following conclusions can be drawn regarding the effect of chemical and mechanical weathering in the weak rock cut slope:

- In the cut slope, chemical weathering existed before the excavation of the slope in the upper part. Physical weathering occurred after the excavation. Both chemical and physical weathering progressed in the intact nonweathered mudstone in the direction perpendicular to the cut slope surface with time. The upper part of the slope is more chemically weathered compared to the lower part of the slope. Physical weathering was comparatively uniform in all the parts.
- The oxidation zone in the lower part of the slope is expected to become up to 2.5 – 3.0 m below the surface in the future and have a more uniform profile of weathering all over the slope. Dissolution will continue below the oxidized zone.
- Reduction in strength of the slope occurred up to 2.5 – 3.0 m below the surface of the slope and a further reduction in strength is expected in this depth.
- The stiffness of the slope is reduced with time after excavation. The significant reduction occurred at the depth up to 2.5 – 3.0 m below the surface of the slope. The stiffness of the overall slope is expected to reduce more in the future.
- The suggested accelerated chemical weathering method was successful in initiating the chemical weathering process in the mudstone and the field conditions could be observed in the laboratory.
- The disappearance of pyrite and the reduction of the pH of the mudstone is closely linked. The direct relationship between pyrite reduction and pH change from alkaline to acidic with acid volume could be obtained from this test.

- Both current in situ pH and mineralogy of the mudstone are important indicators of the chemical weathering state. However, mineralogy gives more useful information in this matter compared to pH.
- High repeatability of the accelerated weathering test was confirmed with mudstone from two different locations; hence this test method is valid for the mudstone from other locations and geology as well.
- With the reduction of the strength in the depth of 3.0 m below the surface of the slope, the critical failure surface of the slope will change and can induce a landslide of the oxidized zone in about 200 years. The factor of safety of the slope will become 1 after 500 years due to weathering.
- The proposed simplified analytical method can predict a similar outcome as the RPFEM model. Hence it can be successfully used as an alternative to the RPFEM model.

Limitations and recommendations of the study

- In this study, the effect of temperature variation and extreme weather conditions was not considered. The effect of the water table also needs to be studied further.
- An accelerated weathering test should be developed to find the connection between chemical and mechanical weathering.
- In this research, accelerated weathering tests were conducted for pH 2 which is an extreme condition. Tests with other mild pH such as pH 3 or pH 4 should be conducted.
- Checking the variation of the strength properties during accelerated weathering should be included.
- During modelling, only variation of cohesion of the mudstone was considered while the angle of friction was kept constant. There is a great scope of research for the future to incorporate variations of the angle of friction with weathering. Combining these features, this study can be modified to get better results.
- From this research, it was well understood that the initiation of chemical weathering from the exposure of the mudstone in the environment plays a major role in the final degradation of the slope surface. Hence if the surface weathering rate can be lowered, the overall degradation of the slope can be delayed. For this purpose, to protect the surface and delay the rate of chemical weathering, a few steps are recommended which are:
    - Removal of the weathered surface.
    - Covering the slope surface with vegetation/vegetation mat/ combination of waste tyres and vegetation.
    - Covering the slope surface with geosynthetics.
    - Applying shotcrete to the exposed slope where the weathering and the probability of slope failure are high.

References

Bhattarai , P., Marui, H., Tiwari, B., Watanabe, N., & Tuladhar, G. (2007). Depth-wise variation of physical and mechanical properties of mudstone in relation to weathering. *Journal of the Japanese Landslide Society*, 79-89.

Bhattarai, P., Binod, T., & Hideaki, M. (2007). Variation of soil properties in mudstone with depth and its effect on slope stability. *Geo-Denver 2007, New Peaks in Geotechnics.* Denver, Colorado.

Bishop, A. W. (1955). The use of the Slip Circle in the Stability Analysis of Slopes. *Géotechnique*, 7-17.

Brunsden, D., & Prior, D. (1984). *Slope instability.* Wiley, Chichester: M. J. Selby.

Carroll, D. (1970). *Rock Weathering.* New York: Plenum Press.

Chigira, M. (1990). A mechanism of chemical weathering of mudstone in a mountainous area. *Engineering Geology, 29*, 119-138.

Chigira, M. (1993). Dissolution and oxidation of mudstone under stress. *Canadian Geotechnical Journal*, 60-70.

Chigira, M., & Kenji, S. (1987). *Mechanism of chemical weathering of mudstone. Weathering under the natural condition and slope stability. Deigan no kagakuteki fuka no mechanism. Shizen Kankyoka deno fuka to shamen antei.* Japan: N. p.

Chigira, M., & Oyama, T. (1999). Mechanism and effect of chemical weathering of sedimentary rocks. *Engineering Geology, 55*, 3–14.

Chigira, M., & Sone, K. (1991). Chemical weathering mechanisms and their effects on engineering properties of soft sandstone and conglomerate cemented by zeolite in a mountainous area. *Engineering Geology*, 195-219.

Ciantia, M. O., Castellanza, R., & Crosta, G. B. (14 January 2015). Effects of mineral suspension and dissolution on strength and compressibility of soft carbonate rocks. *Engineering Geology*, 1-18.

Ciantia, M., Riccardo, C., & Claudio, D. (2013). Chemo-mechanical weathering of calcarenites: Experiments & theory. In *Coupled Phenomena in Environmental Geotechnics.* London: aylor & Francis Group.

Cripps, J. C., & Czerewko, M. A. (2017). The influence of diagenetic and mineralogical factors on the breakdown and geotechnical properties of mudrocks. *Geological Society*, 271 - 293.

Cull, S. (2009). *Rocks and Minerals.* New York: Chelsea House Publishers.

Dixon, J. B., Hossner, L., Senkayi, A., & Egashira, K. (1982). Mineralogical Properties of Lignite Overburden as they Relate to Mine Spoil Reclamation. *American Society of Agronomy, 10*, 169-191.

Eberhardt , E., Thuro , K., & Luginbuehl, M. (2005). Slope instability mechanisms in dipping interbedded conglomerates and weathered marls—the 1999 Rufi landslide, Switzerland. *Engineering Geology*, 35–56.

Emerson, W. (1964). The slaking of soil crumbs as influenced by clay mineral composition. *Australian Journal of Soil Research* , 211 - 217.

Goudie, A. (1986). Laboratory simulation of 'the wick effect' in salt weathering of rock. *Earth Surface Processes and Landforms*, 275-285.

Gratchev, I., & Towhata, I. (2011). Analysis of the mechanisms of slope failures triggered by the 2007 Chuetsu Oki earthquake. *Geotechnical and Geological Engineering, 29*, 695-708.

Hachinohe, S., Hiraki, N., & Suzuki, T. (1999). Rates of weathering and temporal changes in strength of bedrock of marine terraces in Boso Peninsula, Japan. *Engineering Geology, 55*, 29–43.

Hawkins, A. B., & Pinches, G. (1992). Engineering description of mudrocks. *Quarterly Journal of Engineering Geology, 25*, 17-30.

Hawkins, A., Lawrence, M., & Privett, K. (1988). Implications of weathering on the engineering properties of the Fuller's Earth formation. *Géotechnique*, 517-532.

Hayashi, K., Yama, M., & Yoneda, T. (2005). 幌内層泥岩の風化変質 と劣化. *Jour. Japan Soc. Eng. Geol.*, 198-206.

Hou , Y., Chigira, M., & Tsou , C. (2014). Numerical study on deep-seated gravitational slope deformation in a shale-dominated dip slope due to river incision. *Engineering Geology*, 59-75.

Inada, M., Okuzono, S., & Matsui, M. (1994). *Problematic Soils in Japan; Chapter 7 (in Japanese).*

Ivan, G. B., & Ikuo , T. (2011). Analysis of the mechanisms of slope failures triggered by the 2007 Chuetsu Oki earthquake. *Geotechnical and Geological Engineering*, 29, 695–708.

Knopp, J., Steger, H., Moormann, C., & Blum , P. (2022). Influence of Weathering on Pore Size Distribution of Soft Rocks. *Geotechnical and Geological Engineering*, 5333–5346.

Kojima, S., Nozaki,, T., Nagata, H., Tanahashi, R., Kondo, R., Okamura, N., . . . Ohtani , T. (2013). Large-scale landslides in Toyama Prefecture, central Japan, and their probable relationship with earthquakes. *Environmental Earth Sciences*, pages2753–2763.

Koma, T., Yasumoto , S., & Kodama, K. (1983). Forms of sulfur, carbon, chlorine and iron compounds and their depositional environment, in the Kazusa Group, the Boso Peninsula, central Japan. *Bulletin of the Geological Survey of Japan, 34*, 191-206.

Lee, J.-S., & Yoon, H.-K. (2017). Characterization of rock weathering using elastic waves: A Laboratory-scale experimental study. *Journal of Applied Geophysics*, 24-33.

Li, L. C., Tang, C. A., Zhu, W. C., & Lianga, Z. Z. (2009). Numerical analysis of slope stability based on the gravity increase method. *Computers and Geotechnics, 36*, 1246-1258.

Lu, Y., Wang, L., Sun, X., & Wang , J. (2016). Experimental study of the influence of water and temperature on the mechanical behavior of mudstone and sandstone. *Bulletin of Engineering Geology and the Environment*, 645–660.

Marty, N. C., Lach, A., Lerouge, C., Grangeona, S., Claret, F., Fauchet, C., . . . Tremosa, J. (2018). Weathering of an argillaceous rock in the presence of atmospheric conditions: A flow-through experiment and modelling study. *Applied Geochemistry*, 252-263.

Maruto corporation. (2006). *Penetrometer for Soft Rock: Model SH-70 Instruction Manual.* Tokyo, Japan.

Matsumoto, S., Shimada, H., & Sasaoka, T. (2017, May 9). Interaction between physical and chemical weathering of argillaceous rocks and the effects on the occurrence of acid mine drainage (AMD). *Geosciences Journal*.

Merrill, G. P. (1897). *A treatise on rocks, rock-weathering and soils.* New York: The Macmillan company; London, Macmillan & co., ltd.

Moore, D. M., & Reynolds Jr., R. C. (1989). *"X-ray Diffraction and the Identification and Analysis of Clay Minerals".* New York, USA: Oxford University Press.

Muntohar, A., & Liao, H. (2009). Analysis of rainfall-induced infinite slope failure during typhoon using a hydrological–geotechnical model. *Environmental Geology, 56*, 1145-1159.

Ning, L., Yunming, Z., Bo, S., & Gunter, S. (2003). A chemical damage model of sandstone in acid solution. *International Journal of Rock Mechanics & Mining Sciences, 40*, 243–249.

Okamoto , R., Kojima, K., & Yoshinaka , R. (1981). Distribution and engineering properties of weak rocks In Japan. *ISRM International Symposium* (pp. pp. 1269-1283). Tokyo, Japan: International Society for Rock Mechanics and Rock Engineering.

Oyama, T., & Chigira, M. (2000). Weathering rate of mudstone and tuff on old unlined tunnel walls. *Developments in Geotechnical Engineering, Volume 84*, 279-291.

Ping, S., Wang, F., Wang, D., Li, S., Yuan, Y., Feng, G., & Shang, S. (2023). Multi-scale deterioration mechanism of shear strength of gypsum-bearing mudstone induced by water-rock reactions. *Engineering Geology*.

Prandtl, L. (1920). Über die Härte plastischer Körper. *Nachr. Ges. Wiss. Goettingen Math.-Phys. Kl.*, 74-85.

Price, D. G. (2013). Weathering and weathering processes. *Quarterly Journal of Engineering Geology and Hydrogeology*, 243-252.

Pusch, R. (1983). *Use of clays as buffers in radioactive repositories.* Lulea: University of Lulea, Division of Soil Mechanics.

Pye, K., & Miller, J. A. (1990). Chemical and biochemical weathering of pyritic mudrocks in a shale embankment. *Quarterly Journal of Engineering Geology, London, 23*, 365-381.

Ruiz-Vera, V., & Wu, L. (01 November 2006). Influence of Sodicity, Clay Mineralogy, Prewetting Rate, and Their Interaction on Aggregate Stability. *Soil Science Society of America Journal*, 1825-1833.

Russell, D. J., & Parker, A. (1979). Geotechnical, mineralogical and chemical interrelationships in weathering profiles of an overconsolidated clay. *Engineering Geology, 12*, 107-116.

Schieber, J. (1999). Distribution and deposition of mudstone facies in the Upper Devonian Sonyea Group of New York. *Journal of Sedimentary Research, 69*, 909-925.

Senkayi, A. L., Dixon, J. B., & Hossner, L. R. (1981). Transformation of Chlorite to Smectite Through Regularly Interstratified Intermediates. *American Society of Agronomy, 45*, 650-656.

Singh, T., Gulati, A., Dontha, L., & Bhardwaj, V. (2008). Evaluating cut slope failure by numerical analysis—a case study. *Natural Hazards*, 263-279.

Sperling, C., & Cooke, R. (1985). Laboratory simulation of rock weathering by salt crystallization and hydration processes in hot, arid environments. *Earth Surface Processes and Landforms*, 541-555.

Susan, L. B., Molly, E. H., Jin, L., & Bazilevskaya, E. (2013). Probing deep weathering in the Shale Hills Critical Zone Observatory, Pennsylvania (USA): the hypothesis of nested chemical reaction fronts in the subsurface. *Earth Surface Processes and Landforms, 38*, 1280–1298.

Sutton, D., McCabe, B., O'Connell , A., & Cripps , J. (2013). A laboratory study of the expansion of an Irish pyritic mudstone/siltstone fill material. *Engineering Geology*, 194-201.

Tanimoto, C. (1982). Engineering experience with weak rocks in Japan. *The 23rd U.S Symposium on Rock Mechanics (USRMS)* (pp. 999-1014.). Berkeley, California: American Rock Mechanics Association.

Tarbuck, E. J., Lutgens, K. F., & Tasa, G. D. (2014). *Earth: An Introduction to Physical Geology, 11th Edition.* Pearson.

Taylor, R. K. (1988). Coal Measures mudrocks: composition, classification and weathering processes. *Quarterly Journal of Engineering Geology and Hydrogeology,21*, 85-99.

Tran , M., Shin, H., Byun, Y.-H., & Lee, J.-S. (27 January 2012). Mineral dissolution effects on mechanical strength. *Engineering Geology*, 26-34.

Ulrey, A. l., & Drees, L. R. (2008). *"Methods of Soil Analysis, part 5- Mineralogical Methods".* Madison, Wisconsin, USA: Soil Science Society of America, Inc.

Utili, S., & Crosta, G. (2011). Modeling the evolution of natural cliffs subject to weathering: 2. Discrete element approach. *JOURNAL OF GEOPHYSICAL RESEARCH, VOL. 116*, 116.

Veder, C. (1981). *Landslides and their stabilization.* New York: Springer-Verlag.

Vlastelica, G., & Miščević, P. (2012). Time-dependant stability of slopes excavated in marl. *Građevinar*, 64.

Warren, C. L., & Lynn, D. W. (1966). Alteration and Formation of Clay Minerals During Cat Clay Development. *Clays and Clay Minerals.* Berkeley, California.

Weisener, C., & Weber, P. (2010). Preferential oxidation of pyrite as a function of morphology and relict texture. *New Zealand Journal of Geology and Geophysics*, 167-176.

Wen, B., Li, H., & Ke, K. (01 January 2014). Effect of Soaking on Shear Strength of Weathered Argillaceous Rocks Susceptible to Landsliding in the Three Gorges Area of China. *Landslide Science for a Safer Geoenvironment* , 135–140.

Wetzel, A., & Einsele, G. (1991). On The Physical Weathering of Various Mudrocks. *Bulletin of Engineering Geology and the Environment, 44*, 89-100.

Yoneda, T., Hayashi, K., & Kashiwaya, K. (2014). Mineralogical Characterization of Mudstone Weathering: A Case Study in a Landslide Area, Central Hokkaido, Japan. *ISRM International*

Symposium - 8th Asian Rock Mechanics Symposium, . Sapporo, Japan: International Society for Rock Mechanics and Rock Engineering.

Yoshida, N., Morgenstern, N., & Chan, D. (1991). Finite-element analysis of softening effects in fissured, overconsolidated clays and mudstones. *Canadian Geotechnical Journal*, 51-61.

Zheng, Y., Chen, C., Liu, T., Zhang, W., & Yafen, S. (2017). Slope failure mechanisms in dipping interbedded sandstone and mudstone revealed by model testing and distinct-element analysis. *Bulletin of Engineering Geology and the Environment*, 77.

APPENDIX A

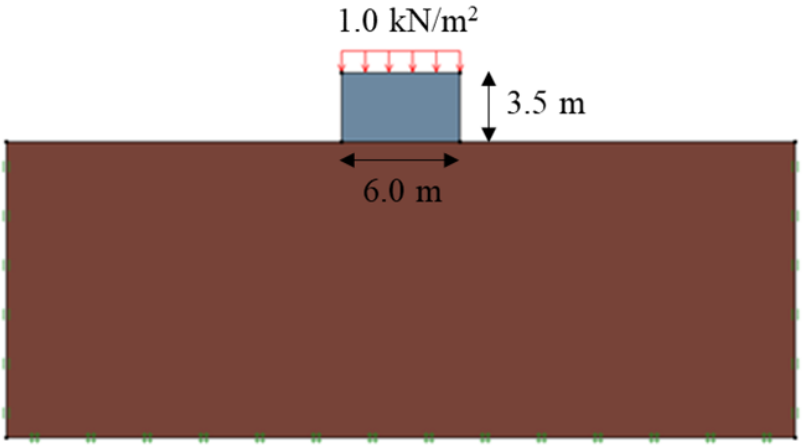

Figure 47 Bearing capacity analysis of soil using Prandtl's theory

The software "Optum G2" was verified by performing bearing capacity analysis using Prandtl's theory (Prandtl,1920). For this, a 6.0 x 3.5 m square footing was placed on the soil (Figure 47). 1.0 kN/m^2 uniformly distributed load was applied on top of the footing. Both the soil and the footing were considered weightless i.e., having a unit weight of 0. The soil block was fully supported at the bottom, hence displacement in all the directions at bottom of the soil was constrained. On the sides of the soil block, normal/roller support was provided. Hence, on the sides, displacement in the normal direction was constrained; displacement only in the upward or downward direction was permitted. The soil was assumed to be purely cohesive. Hence, assuming cohesion (c) value as 30 kN/m^2 and φ value as 0°. Based on all these assumptions, according to Prandtl's theory (Prandtl,1920), the failure surface in the soil must be a circular arc and the bearing capacity of the soil is,

Bearing capacity, $q_u = 5.14\ c = 5.14 \times 30 = 154.2$ kN/m^2

From the simulation using the upper and lower bound principle, the bearing capacity of the soil was found to be 160.131 kN/m2 (upper bound) and 149.719 kN/m2 (lower bound) which encloses 154.2 kN/m2. . The failure surface was also found to be a circular arc. The results are shown in Figure 48. Hence, the software was verified for the slope stability analysis.

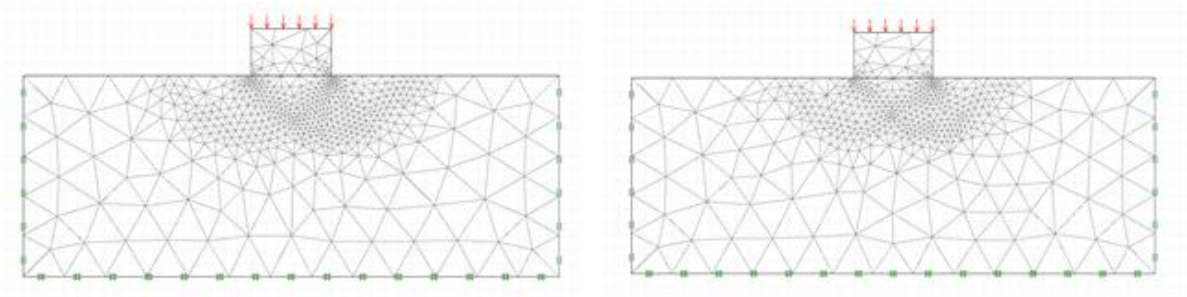

Failure mode of soil

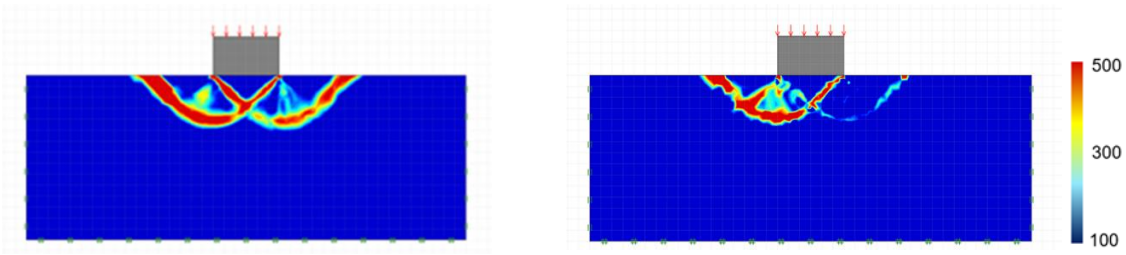

Distribution of plastic multiplier ($\dot{\lambda}$)

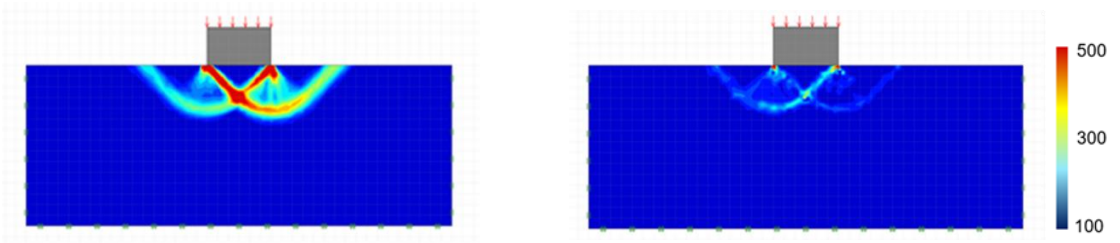

Distribution of residual strain rate ($\dot{\varepsilon}_1$- $\dot{\varepsilon}_3$)

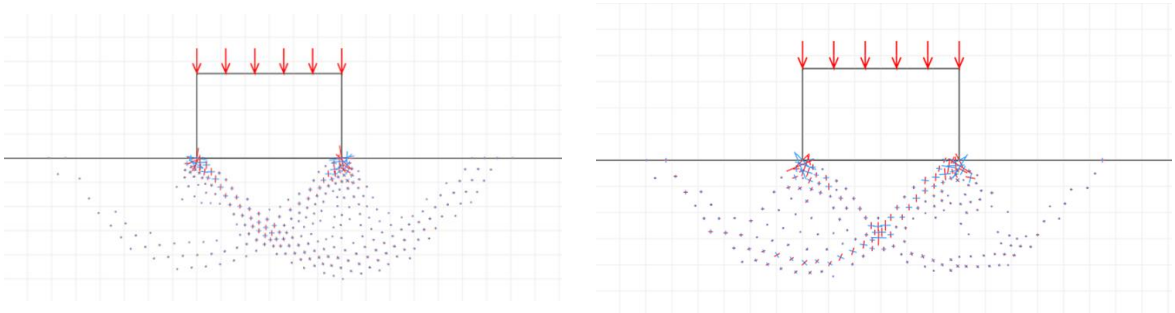

Distribution of strain, $\dot{\varepsilon}_1$ and $\dot{\varepsilon}_3$ vectors

Figure 48 Results of bearing capacity analysis (left: upper bound, right: lower bound)

APPENDIX B

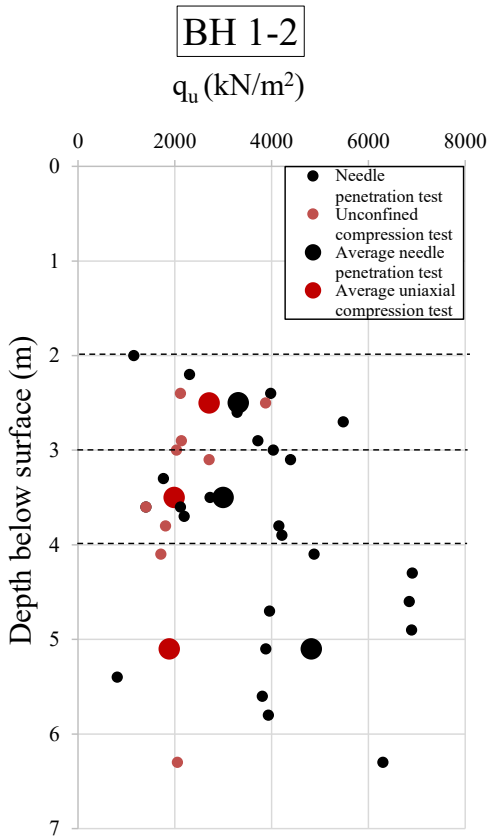

Figure 49 Comparison of needle penetration test with uniaxial loading test results

Comparison of unconfined compressive strength obtained from needle penetration test results and the uniaxial loading test was done by taking the average of both test results separately. Only needle penetration test was conducted in the samples collected from the borehole BH 1-2 until the depth of 2.0 m as the samples collected from this depth were relatively weak and the specimens for the uniaxial loading test could not be formed. Hence, no comparison could be made in this depth. The average of the unconfined compressive strength obtained from the needle penetration test and uniaxial loading test of the samples in the depths of 2.0 – 3.0 m, 3.0 – 4.0 m, 4.0 to 7.0 m are plotted in Figure 47. In 2.0-3.0 m depth, and 3.0 – 4.0 m depth, the average values are close to each other. In 4.0-7.0 m depth, the average values have a big difference mainly due to the scarcity of uniaxial test data.

APPENDIX C

Table 9 Summary table of the results of XRD analysis and pH test of borehole B1 of Zushi